



Maintenance of Near-Surface Stratification in Doubtful Sound, a New Zealand Fjord

M. T. Gibbs^{a,d}, M. J. Bowman^b and D. E. Dietrich^c

^aDepartment of Marine Science, University of Otago, New Zealand

^bMarine Sciences Research Center, State University of New York Stony Brook, U.S.A.

^cCenter for Air Sea Technology, Mississippi State University, U.S.A.

Received 17 September 1999 and accepted in revised form 4 September 2000

The surface waters of Doubtful Sound, a glacially carved fjord in south-western New Zealand, feature a quasi-permanent low-salinity-layer (LSL). The LSL is maintained year round by the extreme precipitation in the catchment ($\sim 7 \text{ m yr}^{-1}$) and discharge from a hydroelectric power station ($\sim 450 \text{ m}^3 \text{ s}^{-1}$). The robust, stable LSL has been shown to play a major role in controlling intertidal and subtidal community structure. By contrast, little is known about the dynamics of the LSL itself. The work presented here elucidates the response of the LSL to perturbations in the wind stress and rainfall.

Frequency-domain analysis of salinity data collected from an array of moored instruments revealed that the LSL responded to perturbations in both the winds and rainfall. However, the specific roles of the wind stress and rain could not be adequately resolved in these analyses. By contrast, simulations of the response of the LSL using a three-dimensional primitive equation model revealed that strong up-fjord directed wind events set up a storm surge at the head of the fjord. This surge significantly deepens the LSL at the head of the fjord and retards or reverses estuarine circulation. The subsequent relaxation of the surge after the abatement of the wind stress resulted in a redistribution of buoyancy throughout the fjord over a two-day period. It is shown that the development and relaxation of the storm surge is a major process controlling the maintenance of the near-surface stratification.

© 2000 Academic Press

Keywords: Fjord; storm surge; low salinity layer; Doubtful Sound; New Zealand coast

Introduction

Oceanographic studies of fjords generally focus on circulation over the whole water-column. Since many fjords consist of interlinked basins several hundreds of metres deep, little emphasis has been placed on the near-surface structure (for example: Gade, 1973; Edwards & Edelman, 1977). However many fjords feature a thin surface layer of brackish water or a low-salinity-layer (LSL) that forms in response to the high precipitation rates common to many fjord catchments (for example Kaartvedt & Svendsen, 1990). Similar freshwater surface layers in shallow estuaries are generally degraded by mixing generated by oscillating tidal currents through the action of bottom boundary stresses. By contrast, the large depths of most fjords minimizes tidal exchange and vertical mixing through the bottom boundary layer, hence fjord LSLs can be very robust throughout the year.

From an ecological perspective, perhaps the most interesting region of fjords is in the near-surface waters since the LSL is often the primary process

^dCorresponding author. Department of Marine Science, University of Otago, P.O. Box 56, Dunedin, New Zealand. E-mail: mgibbs@albers.otago.ac.nz

controlling the vertical structure of rock wall communities (Smith & Witman, 1999). This may be directly through osmotic stresses or indirectly through enhanced light attenuation in the LSL. Although the role of LSLs in controlling ecological processes has been investigated (for example, Kaartvedt & Svendsen, 1990; Witman & Grange, 1998), there is a conspicuous absence of studies that have sought to describe the variability of a fjord LSL and the roles of the dynamical processes controlling the variability. This represents a conspicuous gap in our understanding of fjord ecosystems. In an attempt to address this issue, a study of the structure, variability and dynamics of an LSL in a New Zealand fjord was undertaken.

Around 200 km of the south-western coastline of the South Island of New Zealand is indented with a system of glacially carved fjords (Figure 1). The system comprises 14 individual fjords that range in length from around 15 km to 38 km. The remote positioning of almost all of the fjords ensures that they contain mostly unaltered marine environments that feature many rare assemblages of rock wall biota (Grange & Singleton, 1988). These environments

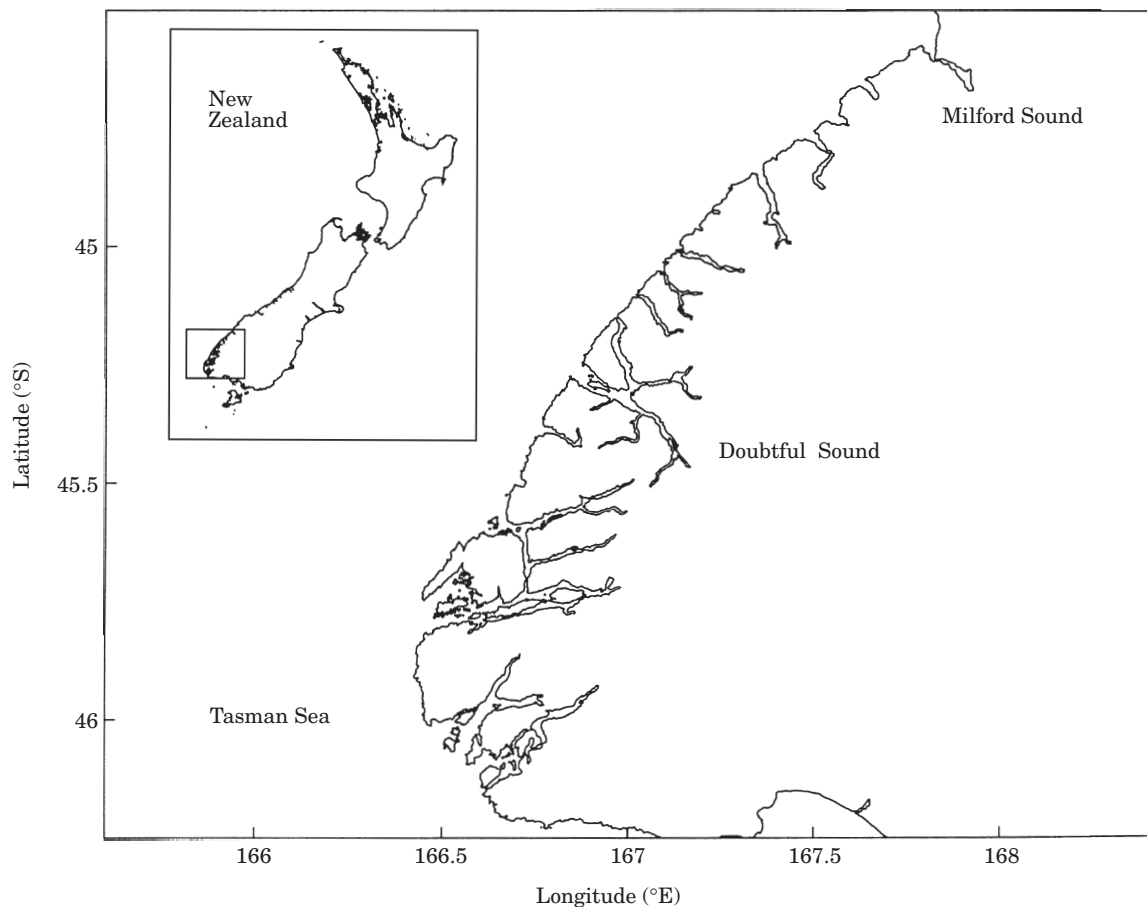


FIGURE 1. Map showing the Fiordland region of south-western New Zealand.

have attracted numerous descriptive studies of the subtidal communities and more recently studies of subtidal ecological processes (Witman & Grange, 1998; Smith & Witman, 1999). This has particularly been the case of Doubtful Sound, one of the central fjords (Figures 1 & 2). A feature of this fjord is the exaggerated LSL, enhanced by the input of fresh water from the discharge of the Manapouri hydroelectric power station at the head of the fjord. The power station routes water from alpine Lakes Manapouri and Te Anau through the power station and into Deep Cove at the head of Doubtful Sound. By contrast to the many biological studies performed in Doubtful Sound, almost no physical oceanographic investigations of the fjord system have been performed. In particular, only the descriptive studies of the hydrography by Stanton and Pickard (1981), Stanton (1986) and McCully (1995) have been published.

In addition, little is presently known about the variability of the LSL in any of the fjords or how the LSLs respond to physical forcing processes. There

are three possible physical processes that are likely to control the depth and structure of the LSL in Doubtful Sound, viz., the discharge from the power station tailrace, rainfall and the wind stress. As noted above, the roles of these processes in controlling this LSL have not been identified despite the considerable importance of the LSL in controlling subtidal assemblages. The influx of fresh water from the Manapouri power station tailrace is typically around $450 \text{ m}^3 \text{ s}^{-1}$, around two to three times more than from catchment runoff, hence the tailrace discharge plays an important role in the maintenance of the near-surface stratification. The response of the Doubtful Sound LSL to winds and rain is less obvious. The only attempts to determine the response of the LSL to the forcing processes were performed by Witman and Grange (1998) and Bowman *et al.* (1999) who sought relationships between the depth of the LSL and rainfall. However in these cases it was assumed *a priori* that the variability was controlled solely by the rainfall or in the study of Bowman *et al.* (1999) by the rainfall and tailrace discharge, despite the potentially dominating

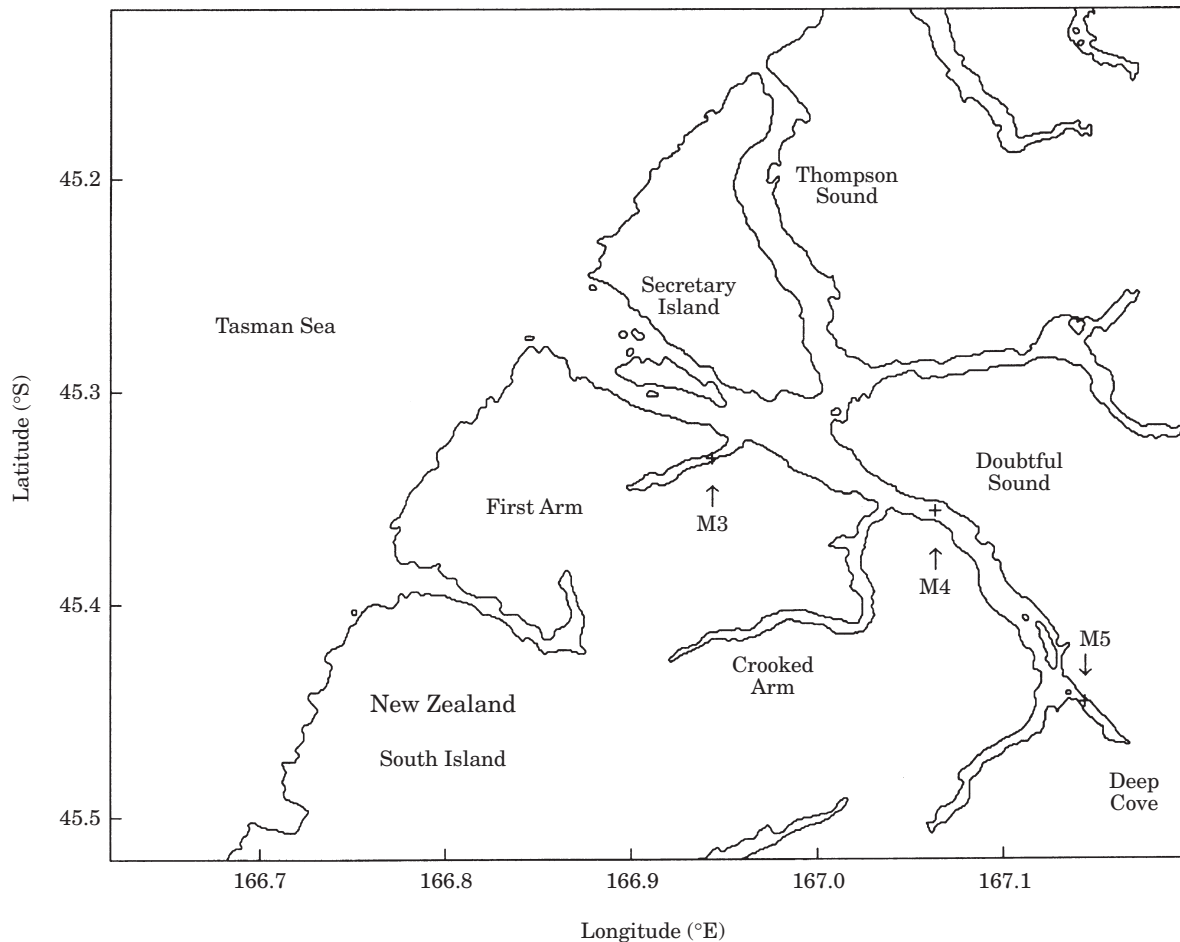


FIGURE 2. Map showing Doubtful Sound and the location of the oceanographic moorings.

influence of the wind stress. In addition, the response of the upper layers of the fjord to the winds and rainfall are potentially very complex. The wind stress acts to vertically mix and therefore destabilize the stratification and redistribute salinity in the vertical. The wind stress may also act to alter the near-surface circulation and hence redistribute buoyancy laterally. By contrast, rainfall acts to stabilize the stratification by adding low density water directly to the sea surface and increasing the horizontal flux of buoyancy from the river runoff as the fresh water advects towards the entrance of the fjord. Second order mixing and entrainment effects result from the velocity shear between the LSL and the underlying marine layer. In addition, strong wind events often coincide with strong rain events, hence the conflicting action of these two forcing processes may act concurrently.

As highlighted above, the importance of the LSL in controlling the assemblages of sub-tidal species, including the rare black corals *Antipathes fjordensis*, has long been recognized (Grange & Singleton, 1988). By

contrast, understanding of the processes controlling the variability in the LSL itself is limited. Hence the principle aim of this paper is to investigate the main sources of variability of the LSL in order to determine in an elementary way the roles of the natural forcing processes associated with the variability.

Data acquisition and preprocessing

The data used here were acquired from moorings (Figure 2) installed for an environmental monitoring programme designed to determine the fate of freshwater introduced into Deep Cove from the Manapouri power station. The moorings collect temperature and salinity data hourly every 2 m from the sea surface down to 21 m, plus at 25 m. The instruments were suspended beneath large surface buoys, hence the depths of the instrumentation are references to the sea surface and not the sea floor. The moorings were named M3 (located in First Arm near the fjord entrance), M4 (located halfway along the

main reach of Doubtful Sound), and M5 (located in Deep Cove at the head of the fjord). The Deep Cove mooring also features a downwards looking Sontek Acoustic Doppler Profiler (ADP) moored on the surface buoy. The ADP bin size is 1 m and the top bin is centred at a depth of 2.5 m. The discharge from the tailrace in Deep Cove is in the form of a narrow (<100 m wide) meandering jet. Mooring M5 was positioned to remain in this jet whenever possible. However, this positioning also ensures that the near-surface velocities measured by the ADP will be mostly greater than the mean flows across Deep Cove since the width of the jet is small by comparison with the width of the fjord.

Wind speed, direction and rainfall data from Deep Cove were acquired from a meteorological station also operated under the monitoring programme. The steep topography and lack of access around the head of the fjord placed significant restrictions on the site availability for this station. This resulted in the station being located in a cove sheltered from winds from some quarters. The steep topography of the walls of the fjord ensures that winds are almost exclusively aligned in the along-fjord direction. In addition, strong wind events are almost always associated with either pre-frontal or post-frontal events, both of which result in onshore/up-fjord winds. Wind data were also acquired from a meteorological station operated by NIWA (National Institute for Water and Atmosphere Ltd., New Zealand) located on Secretary Island near the fjord entrance (Figure 2). These data were used to estimate the sheltering effect of the site of the station in Deep Cove. The maximum zeroth lag correlations between the along-fjord winds at the two sites was found when the magnitude of the Deep Cove winds were multiplied by a factor of 3.6. As a result of these differences, both sets of wind data are used in the analyses presented here. Wind vectors were rotated to align them with the local principal along-fjord and across-fjord directions. Time series of wind stresses were then calculated using the method of Large and Pond (1981). The currents measured by the ADP were also aligned to the local along and across-fjord directions.

Variability and forcing of the LSL

Firstly consider the observed variability in the LSL. Time series of salinity at particular near-surface depths at moorings M5, M4 and M3 are shown in Figures 3, 4 and 5 for the observation period 13 October 1998 to 16 November 1998. Consider first the data from M5 in Deep Cove (Figure 3). The salinity at 1 m is always very low (mean=3.1). By

contrast, at 3 m and 5 m depth the salinity alternates from almost 0 to 32. The salinity at 9 m depth was mostly the oceanic value of around 34–35 with the exception of several periods where the salinity dropped to almost zero. The meteorological data shown in Figure 6 shows that these events on days 292 and 298 coincided with strong wind and rain events. The salinity at 1 m at mooring M5 also shows a clear high frequency signal of ~12 h period. The moorings cannot directly measure sea surface excursions since they are referenced to the sea surface, hence these oscillations in the 1 m salinity data are likely to be either the result of a baroclinic tide or an interaction between the barotropic tide and the tailrace jet.

The salinity at 1 m depth at mooring M4 was generally larger in magnitude (mean=8.9) than at the same depth at M5 (Figures 3 and 4). In addition there were periods when the salinity achieved close to oceanic values (20 to 35), for example during days 287, 292 and 298. These events also coincided with strong wind events at both Deep Cove and Secretary Island for days 292, 298 and Deep Cove winds for day 287 (Figure 6). The salinities below a depth of 7 m were mainly oceanic values with the exception of particular events when the salinities dropped significantly. Once again, these events coincided with periods of strong winds and rainfall (Figures 4 and 6).

The 1 m salinity at mooring M3 was generally greater (mean=13.6) by comparison with the sites further up the fjord (Figure 5). In addition during the periods of strong winds and precipitation the salinity increased more and for a longer period by comparison with M4. The salinity at 5 m depth was predominantly of oceanic values, never less than 17. The M3 salinity at 11 m was always greater than 32 for the whole observational period, indicating that the LSL had little influence at this depth.

The perturbations in the near-surface salinity field are likely to be a response to the individual and combined actions of three forcing processes: wind stress, precipitation and tailrace discharge. The input of freshwater from precipitation may be in the form of rainfall or snow melt. Note that the terms precipitation and rainfall are interchanged here since it is assumed that weather-band perturbations in the natural sources of freshwater arise from the extreme rainfall (around 7 m yr^{-1}).

Wind stress data were acquired from both the head of the fjord (Deep Cove, Figure 6) and near the entrance (Secretary Island; Figure 2). Most of the strong wind events can be seen at both sites, for example during days 292, 298 and 311; however the magnitudes varied between sites. These differences

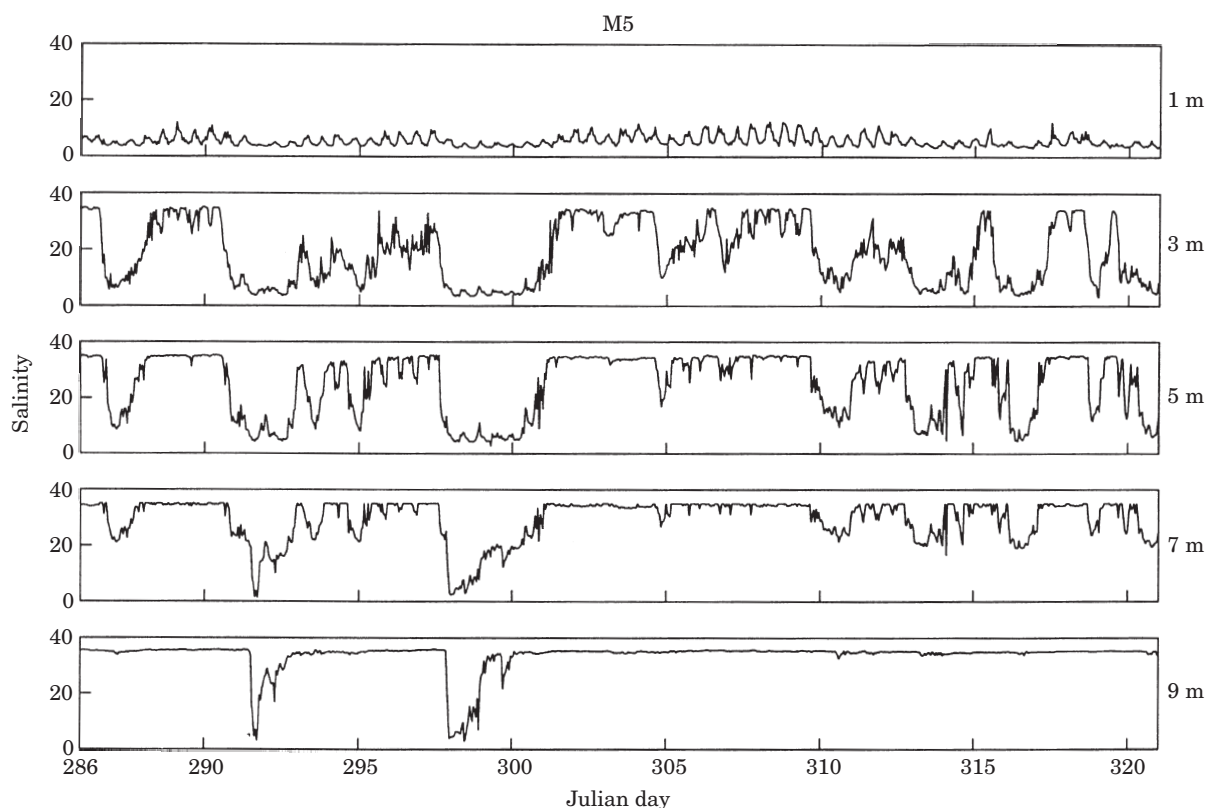


FIGURE 3. Time series of near-surface salinities from mooring M5.

in magnitude may result from sheltering of the instruments, as discussed previously, or real differences resulting from local orographic influences. The mean wind stress for Secretary Island and Deep Cove was 0.05 and 0.03 Pa respectively although the maxima were 0.65 and 0.75 Pa respectively. Both sets of wind stress data exhibit a significant level of high frequency variability. This is to be expected at the Deep Cove site since it is located ~ 30 km inland from the coast and hence will be subjected to strong diurnal changes in atmospheric stratification. The strong high frequency variability at the Secretary Island site (Figure 2) is less expected as this site is located on the coast. Interestingly, there were periods of significant winds (~ 0.1 Pa) at Deep Cove that were not recorded at Secretary Island (Figure 6). Since most of the strong wind events blow onshore (west to east), it is possible that these events recorded only at Deep Cove were a result of very localized processes, for example katabatic winds. Unfortunately details of many of the local meteorological processes are at present unknown, hence conclusive identification of these processes cannot be determined.

The rainfall (mm hr^{-1}) measured in Deep Cove is shown in Figure 6. Most of the strong rainfall events coincided with strong wind events, for example on

days 292 and 298; however, there were periods of strong winds when no precipitation occurred, for example between days 304 and 310. The total rainfall for the period was 202 mm and since the mean rainfall for the region is around 7 m yr^{-1} , the observation period represented a period of relatively low rainfall. The maximum rate of precipitation was 25.6 mm hr^{-1} and occurred during the strong wind event on day 298.

The bottom frame in Figure 6 shows the along-fjord component of the velocity at a depth of 2.5 m. A signal of the semi-diurnal period may be seen in this time series. The ADP measured the total current field hence these oscillations may be associated with both barotropic and baroclinic tides. The strongest events were outflowing currents that generally commenced 1 to 2 days after the onset of the wind events.

The tailrace discharge for the data period is shown in Figure 7. These data show that the input of freshwater into Deep Cove from the tailrace was almost constant at 450 m³ s⁻¹ for the whole period except for during day 320 when it dropped to 320 m³ s⁻¹. This immediately suggests that the perturbations in the observed salinity field (except around day 320) were not associated with a fluctuation in power station discharge.

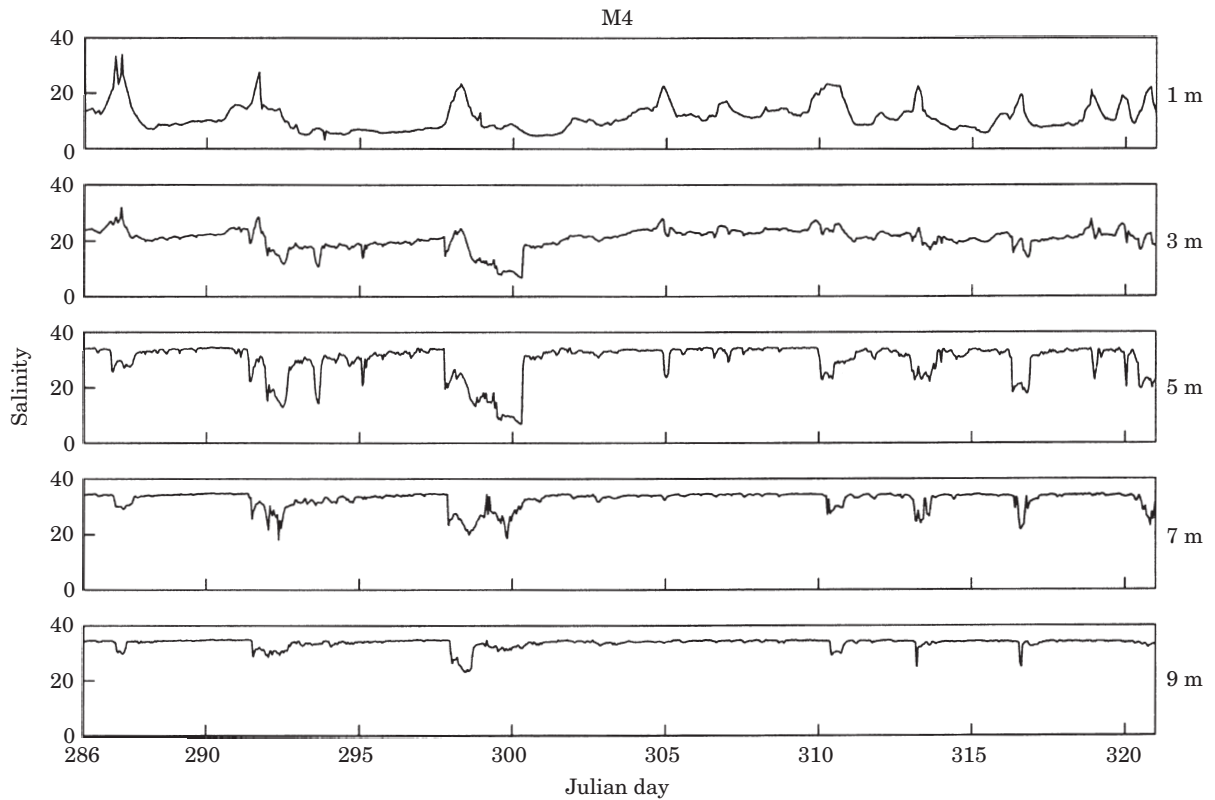


FIGURE 4. Time series of near-surface salinities from mooring M4.

Stratification indices

The data presented in the previous section reveal that large perturbations in the LSL occurred during times of strong wind and rainfall. The tailrace discharge was almost constant during the observational period hence relationships between the natural forcing processes and the response of the LSL will be sought. The stratification in the upper part of the water-column must be quantified prior to any further analyses. An appropriate way to quantify the stratification is to determine the potential energy anomaly (φ), following Simpson *et al.* (1978) and Simpson and Bowers (1981). This quantity represents the energy per unit volume required to homogenize a stratified section of the water column with mean density $\bar{\rho}$, and may be calculated as follows;

$$\varphi = \frac{g}{H} \int_{-H}^0 (\bar{\rho} - \rho(z)) z \times dz \quad \text{J m}^{-3} \quad (1)$$

Where the z co-ordinate is positive vertically upwards from the sea surface and g is the gravitational acceleration. In a fully homogenous water column $\varphi=0$ and $\varphi>0$ under conditions of stable stratification. The advantage of using this quantity is that the stratification can be represented by a scalar parameter.

However, any information about the vertical rate of change of density in the water-column (dp/dz) at particular depths is lost. This calculation also assumes that contributions from advection are minimal (Simpson & Bowers, 1981). Since the currents at mooring M5 were significant, this assumption may be invalidated. However, since the tailrace discharge is constant during the observation period it will be assumed that contributions from horizontal advection of buoyancy will be constant although unresolved. Hence, quantitative comparisons of φ between moorings will not be performed.

Values of φ for each time step at moorings M3, M4 and M5 were calculated for the top 10 m of the water-column (Figure 8). Perhaps the most noticeable feature evident in Figure 8 is the reduction in the mean φ along the fjord, hence the stratification reduces in the along-fjord direction. At M5, 2 periods of full homogenization ($\varphi \sim 0$) occurred around days 292 and 298. Inspection of the wind and rain data shows that both strong wind and heavy rain events occurred on these days (Figure 6). The same homogenizing events can be seen in the estimates of φ from M4 and M3. Additional mixing events occurred at M4 and M3 on days 288, 305, 311, 313 and 317. The events on days 288 and 305 corresponded with

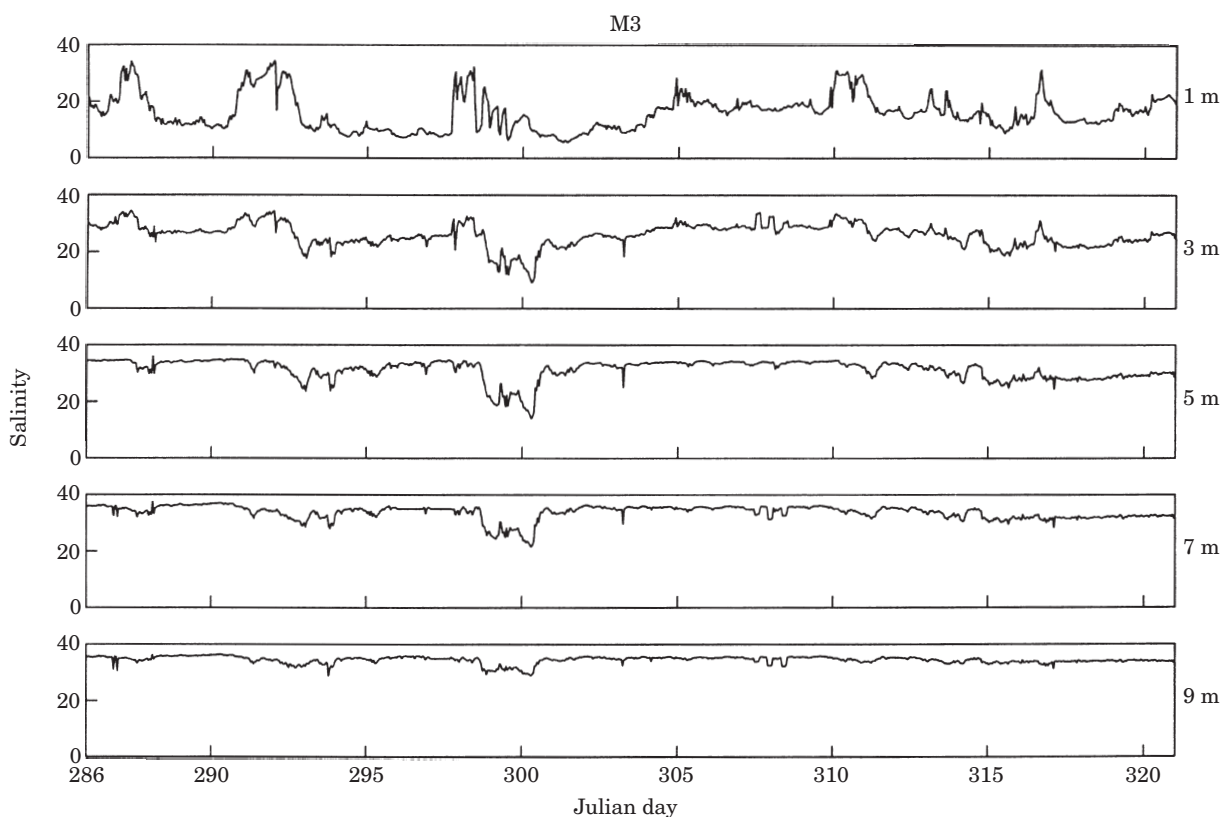


FIGURE 5. Time series of near-surface salinities from mooring M3.

strong wind events although no rainfall was recorded on these days. By contrast, both winds and rain occurred on the other days. The φ values at M5 indicate that an overall increase in stratification occurred during these days near the head of the fjord. However, inspection of the salinity data from M5 (Figure 3) shows that some homogenization did occur over the top 5 m although this mixing did not fully mix the top 10 m, hence an increase in stratification occurred over the depth range 5–10 m.

Another enlightening quantity that may be calculated is the equivalent freshwater depth (*EFD*; Bowman, 1978), as follows;

$$EFD = -z_0 + \int_0^{-z_0} \frac{\rho(z)S(z)}{\rho_0 S_0} dz \quad (2)$$

where z_0 is the depth of the underlying oceanic reference layer of salinity S_0 and density ρ_0 . The values of the *EFD* using a reference salinity of 35 were determined for every hour at moorings M5, M4 and M3 (Figure 9). Comparison of these data shows that the volume of fresh water per along-fjord distance decreased towards the entrance to the fjord. The mean *EFD* over the whole data set at moorings M5,

M4 and M3 were 3.7, 2.5 and 0.7 m respectively. This can be almost completely explained by the widening of the fjord, from around 600 m at M5 to 1100 m near M4 and around 2100 m in the main Doubtful Sound channel at the entrance of First Arm.

The most striking features in the *EFD* data are the events on days 292 and 298 when the *EFD* at M5 was over 10 m, more than twice the mean depth. The tailrace discharge was constant during these periods, hence increases in *EFD* must be from natural precipitation and/or wind events. Rather than a gradual increase in *EFD* as may be expected from the smoothing effect of retention in the catchment and runoff of the LSL towards the ocean, it appears that the low salinity water is ‘piling up’ in Deep Cove. A pulse of freshwater may be seen exiting the surface of the fjord several days later past mooring M4 and M3 (Figure 9).

Analysis of the variability in the frequency domain

It is clear from inspection of the time series of wind stress, rainfall, φ and *EFD* that there are strong relationships between the natural forcing processes

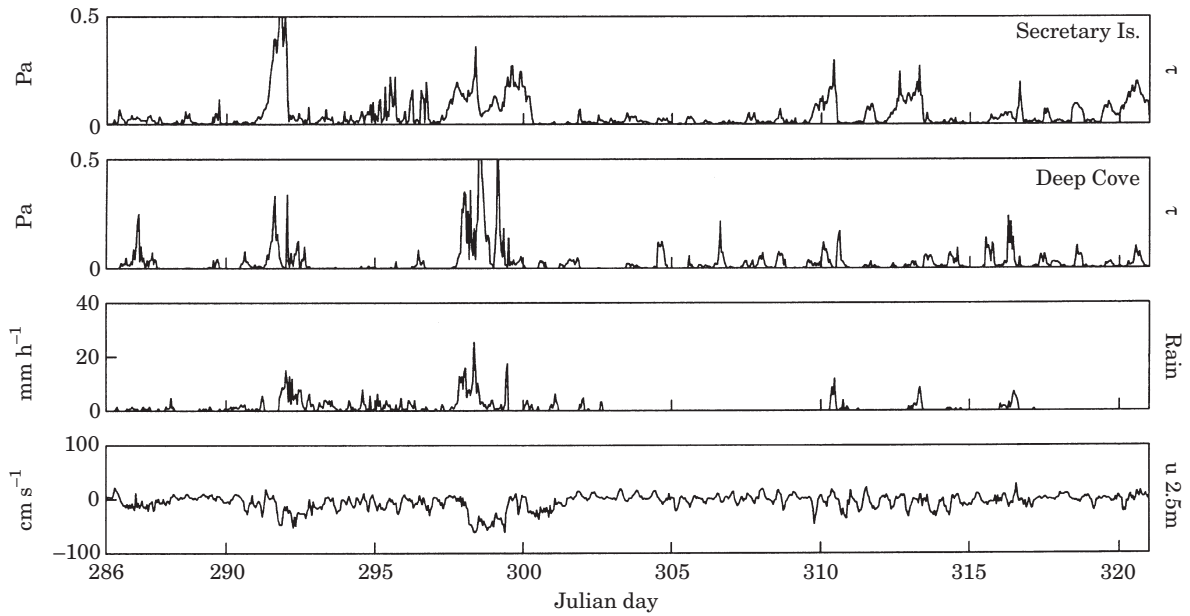


FIGURE 6. Time series of wind stress from Secretary Island and Deep Cove, rainfall from Deep Cove and along-fjord currents at a depth 2.5 m in Deep Cove.

(along-fjord wind stress and rainfall) and the response of the upper stratification (φ and EFD). An analysis in the frequency domain can help to elucidate these relationships.

The power density autospectra of the magnitude of the wind stress at Secretary Island and Deep Cove and rainfall from Deep Cove may be seen in Figure 10(a–c). Generally more energy was associated with the wind stress at Secretary Island [Figure 10(a)] by comparison with Deep Cove [Figure 10(b)] although this may be an artefact of the factor applied to the Deep Cove wind data. In both cases most of the energy resided in bands lower than 0.04 cph (25 h) although the Deep Cove spectra exhibits a broad peak covering the diurnal and semi-diurnal bands. Energy in the diurnal bands is likely to be associated with the diurnal reduction in winds in Deep Cove as a result of increasing atmospheric stratification over the fjord during night hours. By contrast, the spectra of rainfall from Deep Cove is more evenly distributed with the exception of the unresolved peak at 0.004 cph.

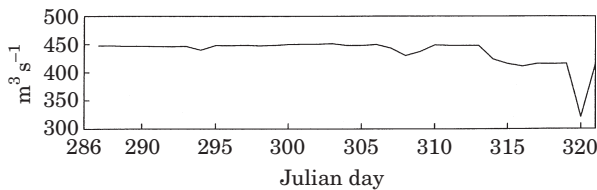


FIGURE 7. Time series of the discharge of fresh water into Deep Cove from the power station.

Comparatively more energy resided in the higher frequencies by comparison with the wind stress spectra.

The autospectra of the near-surface currents in Deep Cove is shown in Figure 10(d). The most noticeable feature here is the well-defined peak centred at the semi-diurnal band (0.09 cph). This is a result of the significant periodic oscillations seen in the data in Figure 3. These are likely to be associated with either the propagation of a baroclinic tide along one of the upper isopycnal surfaces or an interaction of the barotropic tide and the tailrace jet. Further investigation into this process is currently underway and beyond the scope of the present study.

Autospectra of φ at M5, M4 and M3 in addition to the autospectra of EFD at M5 are shown in Figure 11. As may be expected from the wind stress spectra, most of the energy lies in the subtidal bands. The low frequency spectra of φ at M3 [Figure 10(c)] is unresolved as a result of very low frequency motions that may be seen in the time series shown in Figure 5. The only tidal period energy resided in 0.09 cph band in the φ spectra at M5 and this may also be result of the baroclinic tide influencing the very surface stratification.

Squared coherences and phase differences in degrees between the forcing processes and the response of the upper water-column at M5 are presented in Figure 12. The horizontal dashed lines in the squared coherence plots represent the 95% confidence level. Consider first spectral relationships

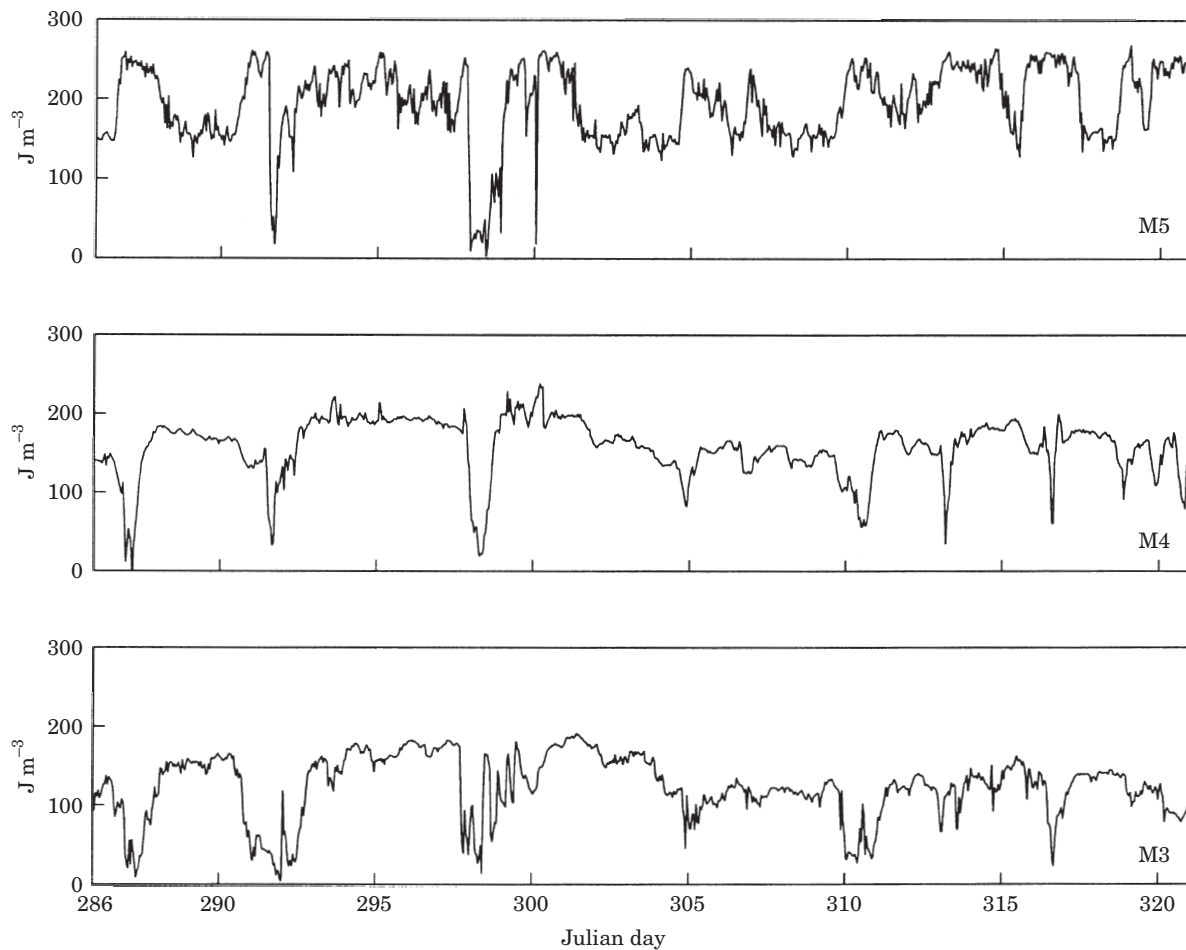


FIGURE 8. Time series of the potential energy anomaly (ϕ) at moorings M5, M4 and M3.

between the Deep Cove wind stress (τ) and the potential energy anomaly (ϕ) at M5. Multiple peaks in the squared coherence spectra below 0.04 cph (25 h) are evident and the phase differences at these frequencies are close to 180° in all cases. This phase difference is to be expected since an increase in τ should result in a decrease in ϕ . A peak at frequency 0.07 cph (around 14 h) is also evident again with a phase difference of 180° . This is probably indicating the response between diurnal changes in stratification and the diurnal wind signal. The latter is associated with the easing of Deep Cove winds as a result of increasing stratification above the sea surface at night. The high squared coherences and consistent phase differences between τ and ϕ at particular frequencies suggests that the wind stress contributes significantly to the variability in the stratification in the top 10 m of the water-column. This may appear to be an obvious result, however, it is still important to highlight this as attempts have been made to predict the stratification in the fjord using rainfall alone (see for example Witman & Grange, 1998).

High squared coherences between the wind stress and *EFD* were also found in the weather bands (Figure 12). For frequencies less than 0.03 cph the phase difference was consistently around 0° , a result that also suggests a strong relationship between these processes. It is not immediately clear why this relationship exists although a possible explanation is that a strong relationship exists between the rainfall and the wind, in which case the wind stress in Figure 6 would be a proxy of rainfall. The squared coherence and phase difference between the Deep Cove wind stress and rainfall may be seen in Figure 13. Strong peaks in the squared coherence spectrum below 0.02 cph and above 0.065 cph indicate that the Deep Cove rain and winds were coupled over several frequency bands. However, the phase difference between the wind stress and rainfall was generally around 180° , which is also surprising.

Inspection of the wind and rain data in Figure 6 reveals that rain events often commence 12–24 h after the onset of the wind events. This is approximately consistent with the phase difference highlighted in the

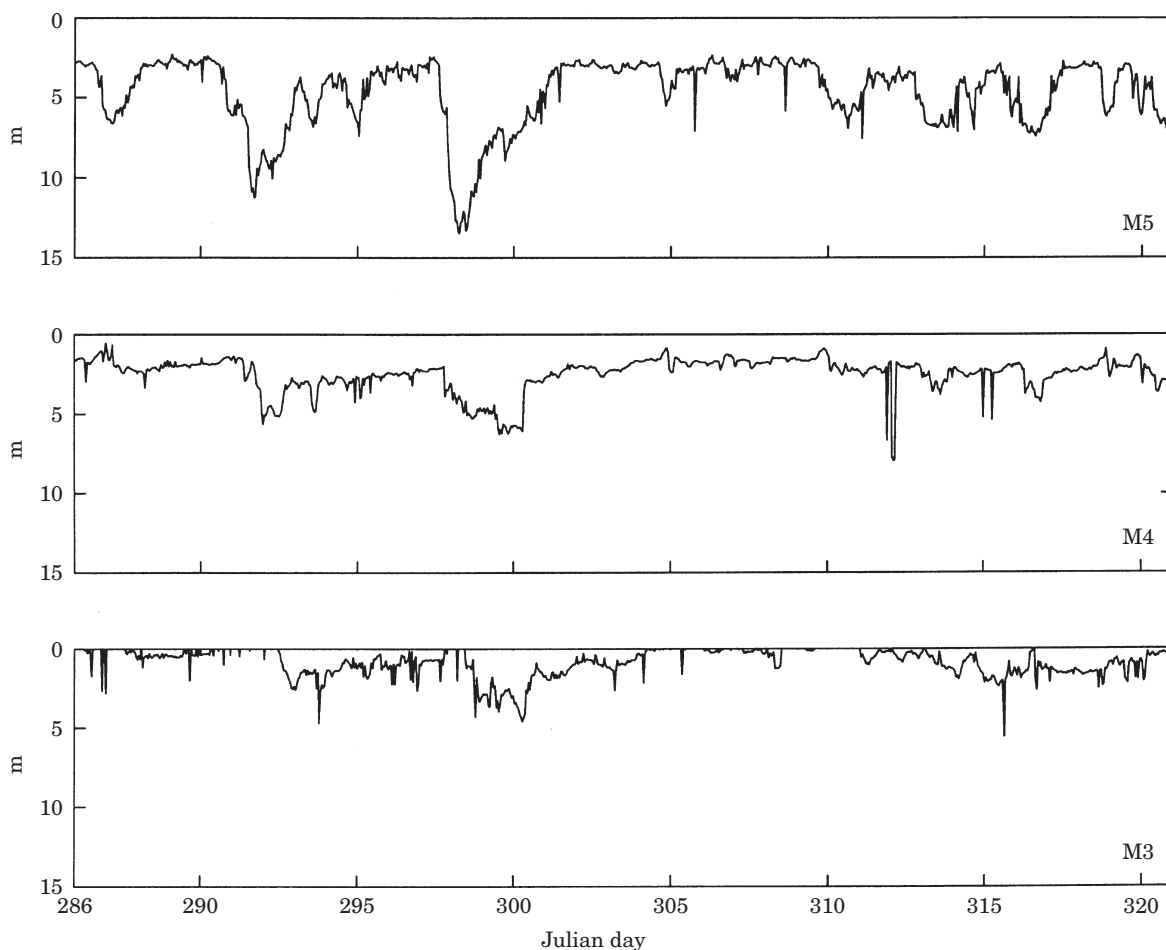


FIGURE 9. Time series of the equivalent freshwater depth (*EFD*) at moorings M5, M4 and M3.

spectral analyses. However, this phase difference cannot adequately explain the negligible phase difference between τ and *EFD* at M5 if the wind stress was acting as a proxy of the rainfall. An alternative explanation for the increase in *EFD* with increased winds would be if the predominantly up-fjord directed winds were 'piling up' freshwater in Deep Cove and reducing the outflow of freshwater into the fjord.

Consider now the relationships between the rain and ϕ in the frequency domain at M5 (lower left frames in Figure 12). Generally only weak relationships were found with the exception of the bands less than 0.015 cph and an isolated peak of high squared coherence of 0.95 at a frequency of 0.049 cph (20.4 h) when the phase difference was almost zero (Figure 12). The anti-phase relationship in the lower bands between the rain and ϕ is unexpected since an increase in rain may be expected to result in an increase in the stratification. By comparison with the weather-band coherences between τ and ϕ , the generally lower weather-band coherences between the rain and ϕ

suggests that the wind stress plays a more important role in governing ϕ than the rainfall over most of the frequency bands.

As expected, high weather-band squared coherences associated with negligible phase difference were found between the rainfall and *EFD* at M5. By contrast, only low squared coherences, less than the 95% confidence interval, were found around the semi-diurnal band (0.08 cph) although the rain spectra showed a peak in this band.

The co-spectral relationships between the winds and ϕ , and rain with *EFD* at M4 may be seen in Figure 14. A consistently strong relationship between the wind stress and stratification is evident over the weather bands at this location. Strong relationships were also found between the rain and *EFD* at M4. Interestingly, phase lags of 0 to 90° are evident. The reason for these phase lags is not known although it suggests that the increase in *EFD* at M4 occurs some time after the rainfall event has commenced.

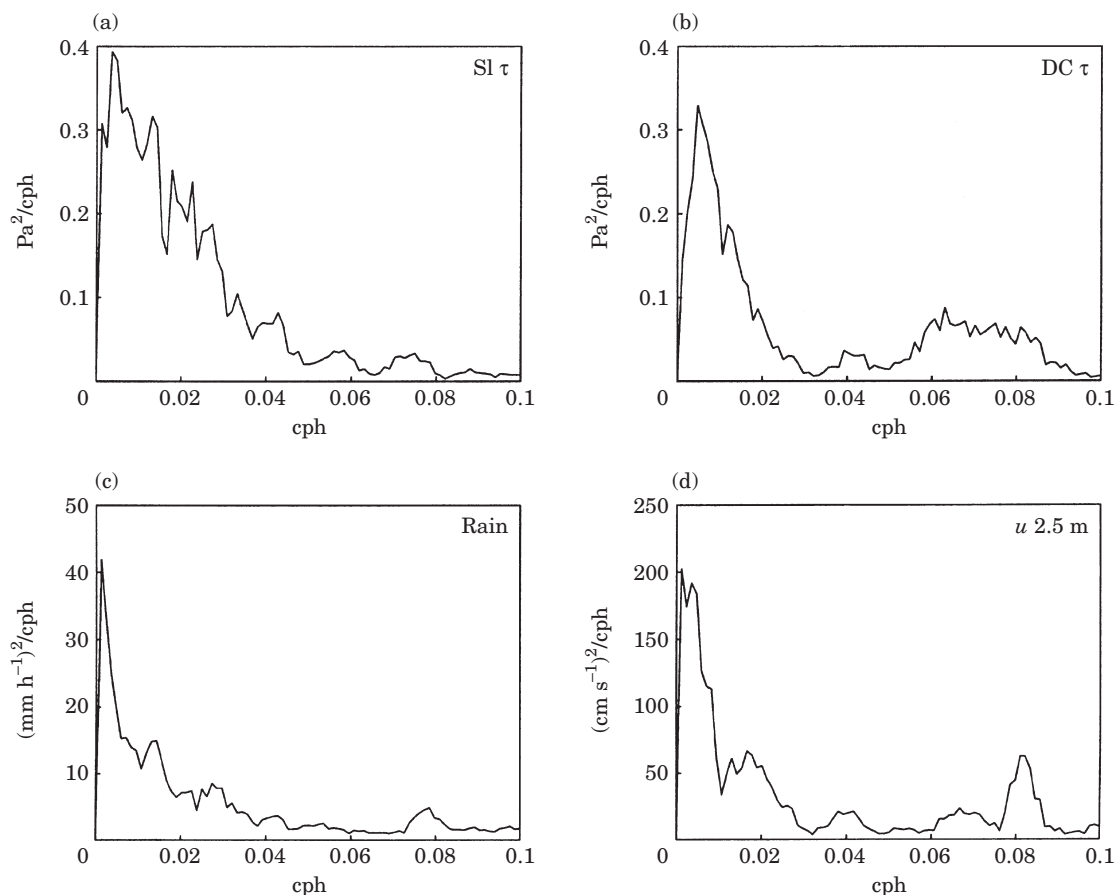


FIGURE 10. Autospectra of the Secretary Island wind stress (a), Deep Cove wind stress (b), rainfall (c) and Deep Cove currents at a depth of 2.5 m (d).

The relationships between the wind stress and φ at M3 are less strong. However this is probably a result of the location of M3 in First Arm, which often has a very different wind regime to the main fjord (pers. obs.).

Strong relationships between the rain and EFD at M3 may be seen. Once again phase lags between 0 and 90° are evident which also suggests that any response of the LSL to increased rainfall occurs sometime after the commencement of the rain events. These phase lags between the rain and EFD at M4 and M5 may be indicating that a pulse of fresh water runs down the fjord after the onset of strong rains. This is in part surprising since runoff enters the fjord from 142 waterfalls and streams distributed along the walls and the retention of the catchment is minimal as a result of the near vertical walls of the catchment.

An analytical mixing model for Deep Cove

The analyses in the frequency domain revealed relationships between the response of the LSL, defined

by φ and the EFD , and natural forcing from wind and rain events. However these analyses also revealed that significant phase lags occur in the responses of the LSL and also that the time series of EFD appears to be related to the wind stress. Hence it appears that the response of the LSL to strong wind and rain forcing is not straightforward. An investigation into the dominant dynamical balances may help elucidate these responses.

An analytical model was developed and applied to mooring M5, near the head of the fjord since this is the only location where velocity data were acquired. Following Nunes Vaz *et al.* (1989) and Rasmussen (1997), we define a model for the rate of change with time of the low-pass filtered potential energy anomaly ($\varphi' = d\varphi/dt$) over the top 10 m of the water-column;

$$\varphi' = \varphi_B' + \varphi_H' + \varphi_P' + \varphi_W' + \varphi_E' \quad (3)$$

The first term on the right hand side of Equation 3 is a horizontal buoyancy flux term. A full explanation of the derivation of this term may be found in Nunes Vaz

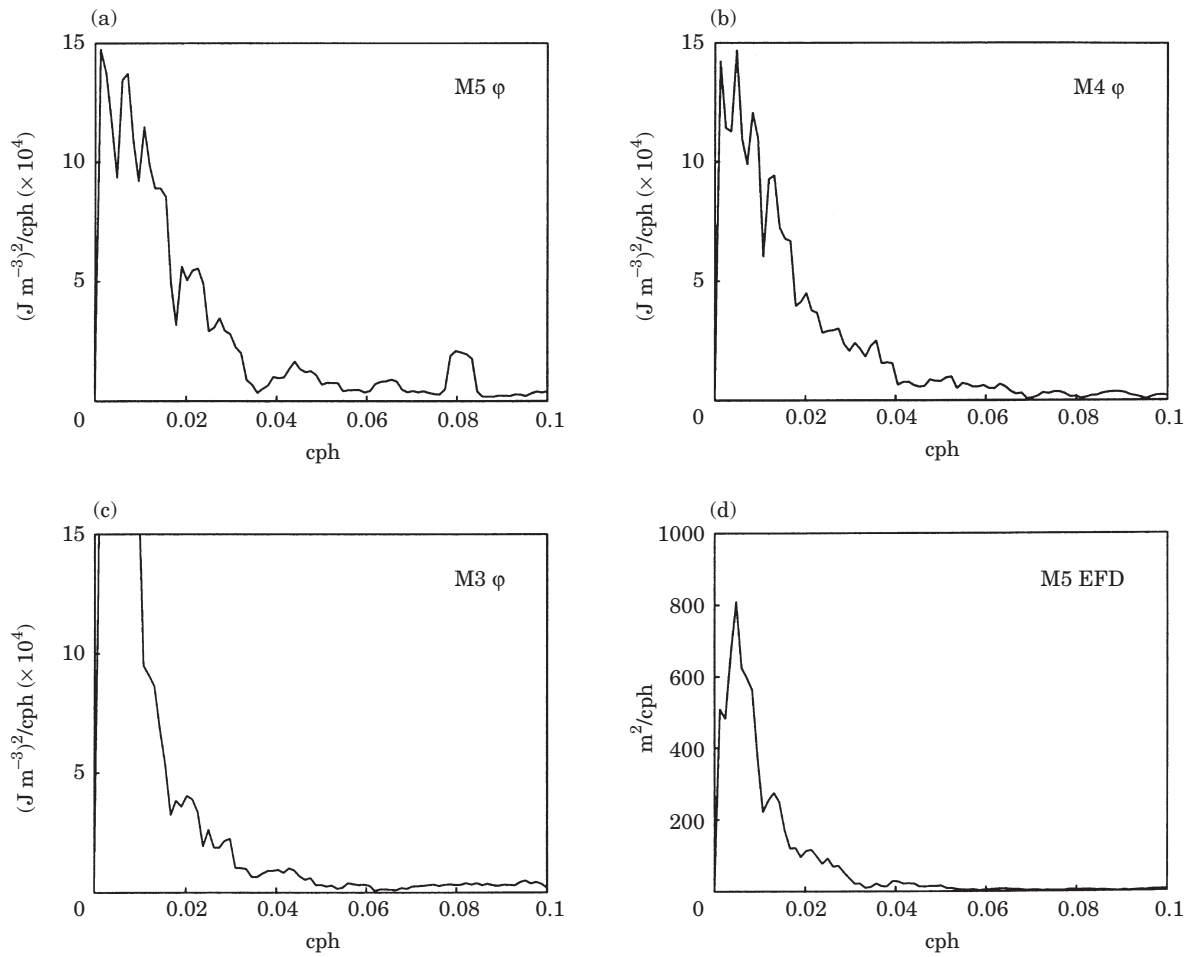


FIGURE 11. Autospectra of the potential energy anomaly (φ) at M5 (a), M4 (b), and M3 (c), and equivalent freshwater depth (EFD) and M5.

et al. (1989). From Nunes Vaz *et al.* (1989) and Rasmussen (1997) we define;

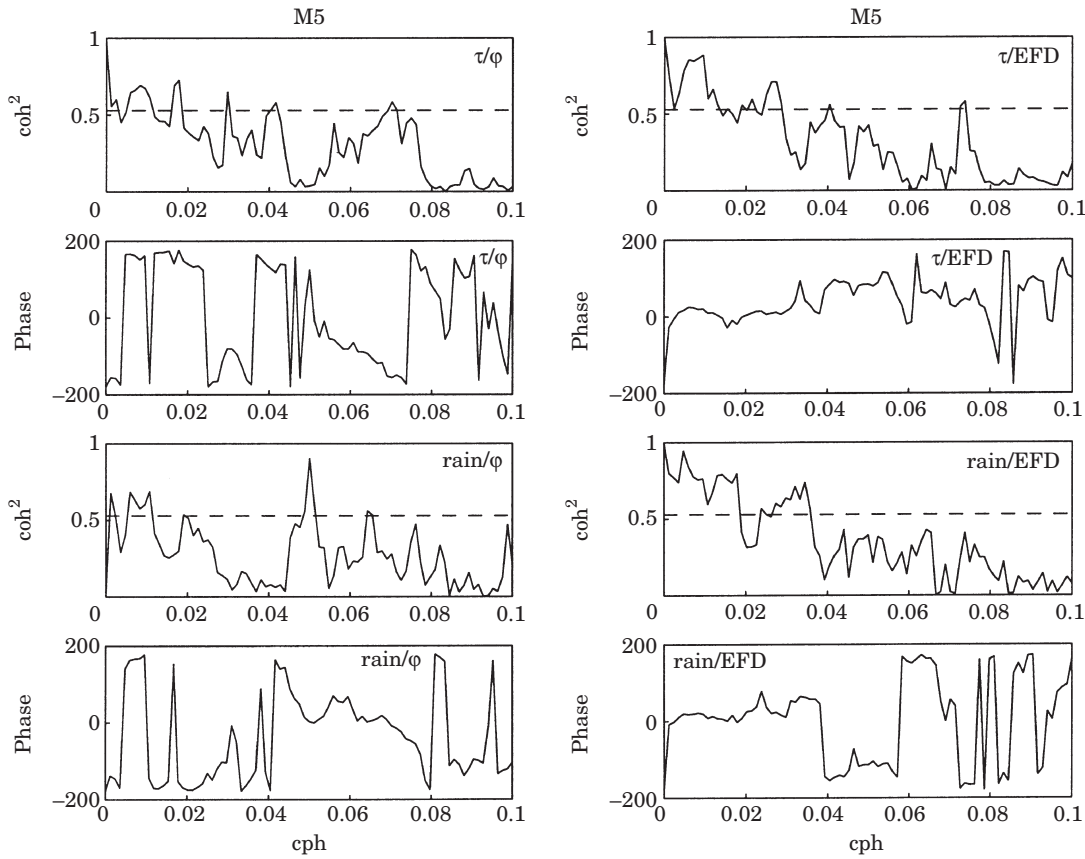
$$\varphi_B' = \beta u_s g H \frac{d\rho}{dx} \quad (4)$$

the parameter β is determined by the vertical structure of the horizontal velocity and can cover a large range of values. Here we assume a linear profile with depth for the horizontal velocity. Thus, following Rasmussen (1997) we set $\beta=1/6$. The gravitational acceleration g and layer depth ($H=10$ m) are constant. The horizontal density gradient ($d\rho/dx$) for each time step was calculated by dividing the difference between the mean density of the top 10 m at M4 and M5 by the horizontal distance between the moorings (12.7 km). Note that it is assumed that this gradient between M4 and M5 represents the local gradient around M5.

The surface velocity (u_s) for every hour was calculated by extrapolating the interpolated velocity profile

acquired from the ADP up to the surface. The ADP top bin was centred at 2.5 m and the bin depth was 1 m below this; it was found that a cubic spline interpolated gave good results for the velocity profile through the top 10 m of the water-column. Unfortunately, as mentioned previously, the ADP data is not particularly representative of the flow in Deep Cove since it usually resides within the jet from the tailrace discharge. However no other near-surface velocity data have been acquired from the fjord as a result of the great difficulty in mooring instruments at depths of less than 2 m in 400 m of water.

The most constraining assumption associated with the use of this parameterization of the horizontal buoyancy flux is the assumption of constant vertical eddy viscosity (Nunes Vaz *et al.*, 1989). This assumption is clearly not valid during conditions of strong stratification. However, initially we assume this term is only significant during periods of strong current at M5 when reasonably well mixed conditions prevailed.


 FIGURE 12. Squared coherence and phase plots between the wind stress, rainfall, ϕ , and EFD at mooring M5.

The second term in Equation 3 is the surface heating term, as follows;

$$\varphi_{H'} = \frac{\alpha}{2 \times C_p} g Q' \quad (5)$$

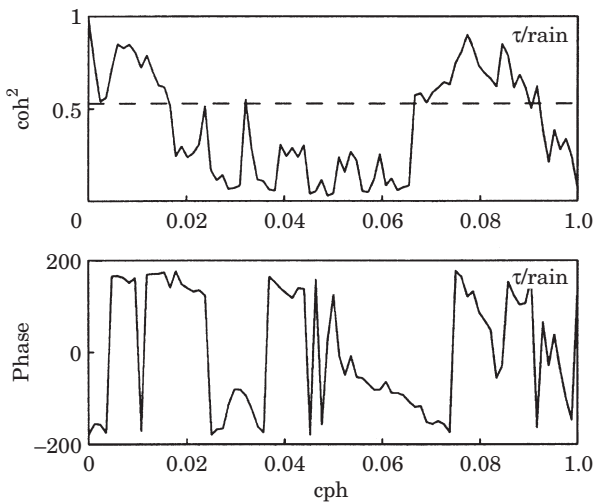


FIGURE 13. Squared coherence and phase between the Deep Cove wind stress and rain.

Here, α is the thermal expansion coefficient and C_p is the heat capacity. Q' is the magnitude of the total surface heat flux. Spectral peaks for the total heat flux commonly concentrate in the seasonal and diurnal bands. Since our data set is less than 5 weeks in length, any seasonal contributions are expected to be small. Both the wind stress at Deep Cove and the M5 salinity at 1 m exhibit diurnal and semi-diurnal contributions. However, since the source of the high frequency contributions in the surface salinities is likely to be baroclinic tides and is only evidenced in the top 2 m, we filter these out by considering only weather-band oscillations. This also implies that the heat flux will make a negligible contribution to φ' , hence we will ignore contributions from this term.

The third term on the right hand side of Equation 3 is the precipitation term $\varphi_{P'}$ where;

$$\varphi_{P'} = \frac{1}{2} g \rho s \gamma P \quad (6)$$

Here s is the salinity of the surface layer, P is the rate of precipitation or rainfall in m s^{-1} and the parameter γ is the coefficient of saline contraction. Rainfall enters

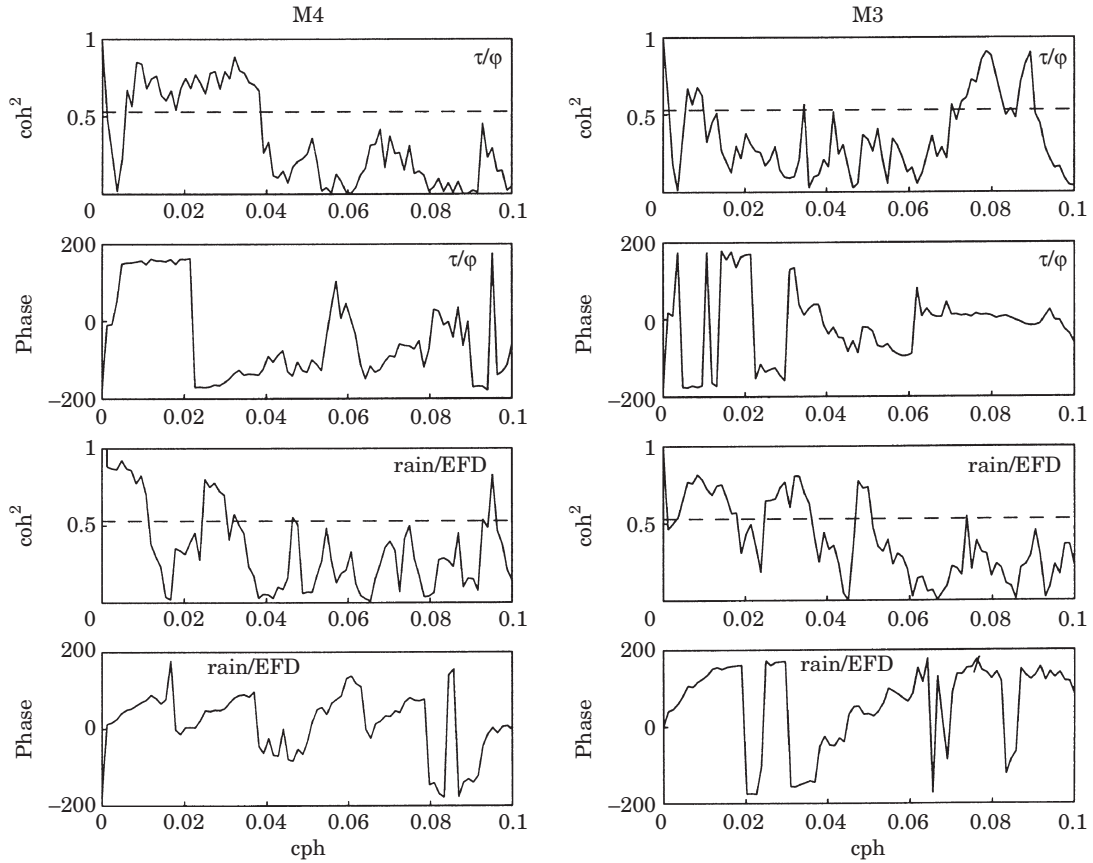


FIGURE 14. Squared coherence and phase plots between the wind stress, rainfall and ϕ at moorings M4 and M3.

the surface from 142 rivers and waterfalls spread around the wall of the fjord. The vertical or near-vertical sides of the catchment also ensure a negligible retention of rainfall on the catchment before it enters the surface waters.

The fourth term in Equation 3 is the first of the mixing terms and describes the redistribution of buoyancy in the water-column as a result of mechanical mixing from the surface wind stress. This is parameterized as follows;

$$\phi_w' = -\frac{\delta\tau}{H} \quad (7)$$

Here τ is the wind stress for each time step and δ is the efficiency of the wind in converting turbulent kinetic energy into potential energy. This simple parameterization of the mixed layer is a weak aspect of the model, however, there is little alternative without resorting to a numerical scheme.

The final term in the model is the entrainment term ϕ_E' . This term describes the destabilization of the base of the LSL as a result of the velocity and density shear between the layers, i.e. it has an approximate

Richardson number dependence. Here we assume that the advection in the lower layer is more than an order of magnitude less than advection in the upper layer (this agrees with the ADP data below 10 m) and parameterize the diapycnal mixing in terms of an entrainment velocity v_e , as follows;

$$\phi_E' = -\frac{1}{2} v_e g \Delta\rho \quad (8)$$

here $\Delta\rho$ is the vertical density contrast between the LSL and the underlying oceanic layer for every hour.

The tunable parameters in the model are the efficiency of the wind mixing (δ) and the entrainment velocity (v_e). An appropriate way to determine these parameters is to choose periods where $\phi' = 0$. For example consider a period when $\phi' = 0$, $P = 0$, and $\tau = 0$, hence Equation 3 becomes

$$\beta u_s g H \frac{d\rho}{dx} = \frac{1}{2} v_e g \Delta\rho \quad (9)$$

assuming $\phi_w' = 0$. This represents a balance between the supply of buoyancy from the tailrace discharge and

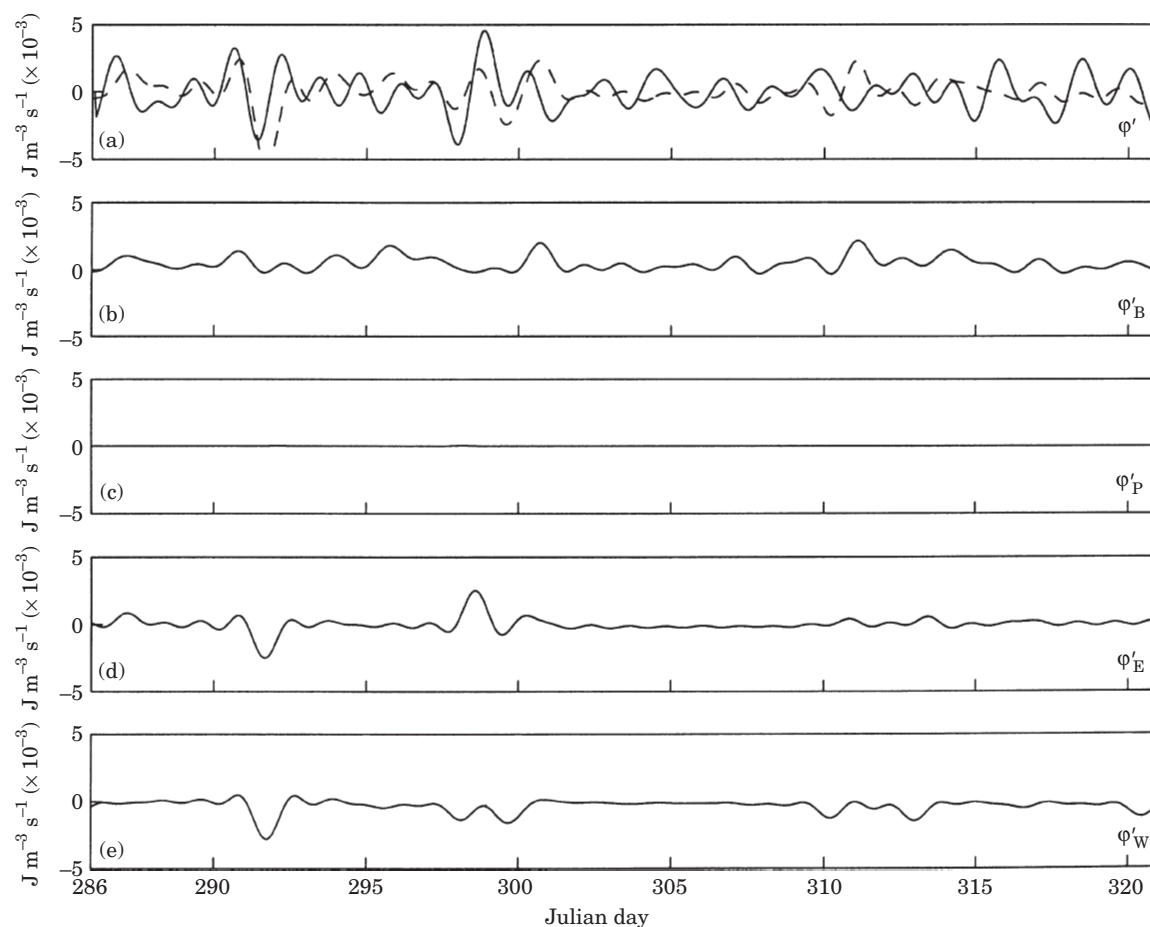


FIGURE 15. Results of the analytical vertical mixing model. The top frame shows the hindcasted (dashed line) and measured (solid line) rate of change of φ . Lower frames show the hindcasted contributions from individual terms, see text for full details.

degradation of the interface from entrainment and diapycnal mixing. By averaging all the values over the period day 301 to 305 inclusive when there was negligible wind and rain, an averaged value of v_e was estimated to be 0.0001 m s^{-1} . Using a constant value for the entrainment velocity represents a significant weakness of this model, however as mentioned previously, it cannot be easily avoided. Comparison of the time series of φ at M5 and Deep Cove wind stress reveals that there were no prolonged periods where $\varphi' = 0$ and $\tau > 0$, hence a similar approach cannot be used to estimate the efficiency of the wind stress. In addition, all of the strong wind events were associated with periods of high rainfall. Hence we must look to the literature for a value of the wind mixing efficiency. The parameter range for this is large and here we use a mid-range value of 0.028, following Nunes Vaz *et al.* (1989).

The results from the model may be seen in Figure 15. The lower frames show the time dependent values of the terms and the dashed line in the top frame shows

the sum of the modelled terms. The solid line in this frame shows φ' determined from the data. Comparison of the solid and dashed lines shows that the performance of the model is best during periods of homogenization of the upper water-column, particularly during the periods centred at days 292 and 298. The agreement between the simulated and estimated φ' during these periods is good. The lower frames in Figure 15 show that the main contributing terms during these events are the entrainment term φ'_E and the wind mixing term φ'_W . During the period centred at day 292, both these terms act to destabilize the water-column although the stratification is restabilized after the event as a result of the resupply of buoyancy (φ'_B). Interestingly, during the period centred around day 298 the entrainment term is acting to stratify the water-column ($\varphi'_E > 0$). This is a result of an unstable density stratification during this period, as may be seen by comparing the salinities at 5, 7 and 9 m in Figure 3.

The agreement between the model and the estimated change in stratification is poorer during the

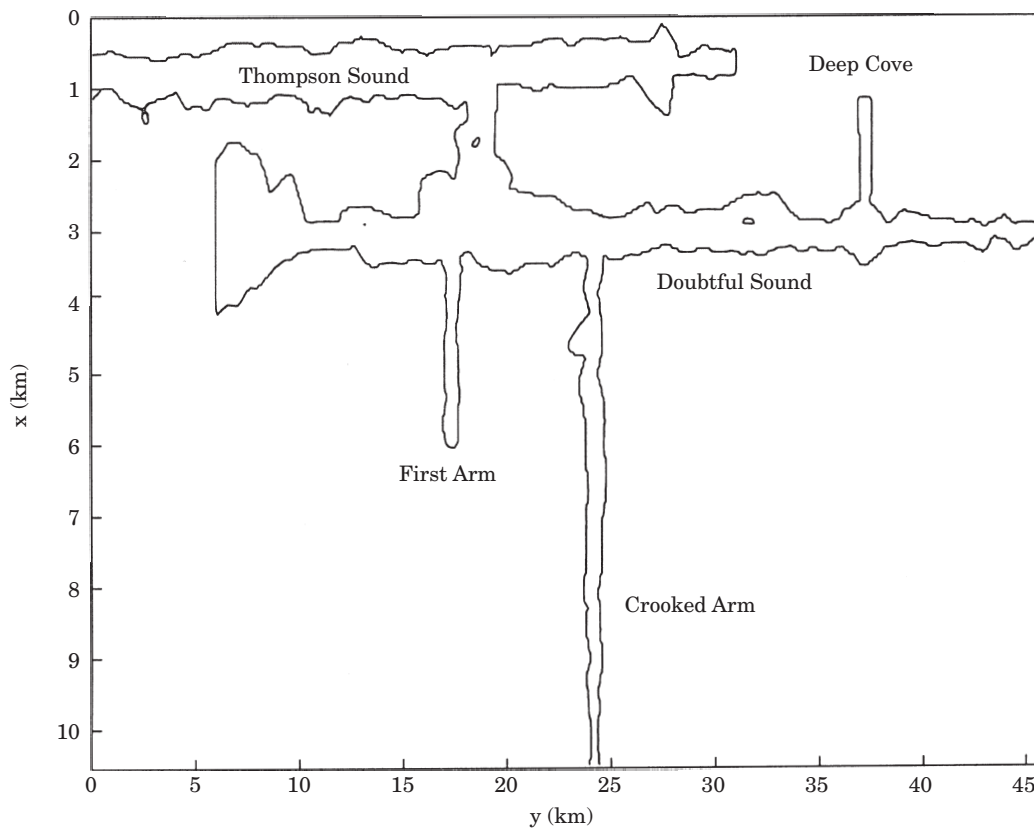


FIGURE 16. Domain of the numerical model. Note that the arms of the fjord have been orthogonalized.

periods of light forcing. Often the model is in anti-phase with the observations. The dominant term during these periods is the horizontal buoyancy flux term ϕ_B' and this is often not balanced by any of the mixing terms. This lack of agreement is likely to be a result of the simple parameterization of the dominant process used here. In particular, the assumption of constant vertical eddy viscosity is not valid during times of high stratification and low ϕ' . The horizontal buoyancy flux term also scales to the ADP velocities that are not representative of the cross-sectional velocities in Deep Cove.

One of the most significant outcomes of the model is the small magnitude of the precipitation term ϕ_P' . The spectral analyses suggested that the rain was a contributing factor in the maintenance of stratification at M5. The discrepancy is likely to be a result of the simple parameterization of the rainfall in the ϕ_P' term. It may also be that the precipitation appears in Deep Cove as increase in discharge from the Lydia River that enters the fjord alongside the tailrace. This river is not gauged hence this cannot be conclusively determined. By contrast, the currents associated with the strong wind and rain events may also be a response to the storm surge created during prolonged periods of

up-fjord winds. Furthermore, although the strongest currents occurred during periods of strong wind and rain, the strongest contributions from ϕ_B' came several days after the abatement of the strong wind and rain events. This suggests there is a 'piling up' of fresh-water in Deep Cove that runs out after the wind has ceased. Although such storm surges have never been accurately measured, anecdotal evidence (including observations by the author) reveal that significant sea level raising occurs during strong wind events.

Numerical simulations of the LSL

The analytical model was able to give some insight into the dynamical balances close to the head of the fjord. However, the application of the model was constrained by the simple parameterization used to describe the vertical processes. In addition the model could not be realistically applied further along the fjord as a result of the lack of velocity data. It is possible using inverse methods to gain an estimate of the velocity structure but this requires assumptions about the relationship between the vertical structure of the water-column and the velocity shear.

An alternative approach is to use a numerical model. A 3-dimensional model constructed around the DieCAST model (Dietrich *et al.*, 1987) was used by Bowman *et al.* (1999) to investigate aspects of the circulation in Doubtful Sound; this model was further developed and used here to investigate the behaviour of the LSL. It must be stressed that the use of the model here was not to fully describe the circulation within Doubtful Sound. This has already in part been performed by Bowman *et al.* (1999) and is currently under further investigation. Rather, the model is used only to investigate the response of the top 20 m of the water column to wind and rain events.

DieCAST is a 3-dimensional rigid lid primitive equation model that uses Z-levels in the vertical. The model is in common use and interested readers are referred to the literature for full details of the numerical methods used by DieCAST. Here we detail only the adaptations required in order to simulate Doubtful Sound.

The Doubtful Sound horizontal grid was orthogonal with each grid cell 200 m square and the fjord arms were orthogonalised to reduce the overall domain size (Figure 16). Twenty grid levels were used in the vertical and these were concentrated in the surface region in order to adequately resolve the LSL. The thickness of the top cell was 43 cm and this increased with depth so that the bottom grid cell was 480 m in thickness. Open ocean boundary conditions were created at the entrance to Doubtful and Thompson Sounds and climatological values of temperature and salinity were maintained at these boundaries. The model was run from rest in a fjord containing climatological hydrography. At the start of the run the tailrace was initialised and 10 days were simulated prior to the onset of wind or rain forcing.

The major enhancements to the model from the work of Bowman *et al.* (1999) are the inclusion of time dependent wind and rain inputs and modifications to the vertical mixing scheme. Precipitation in the catchment is distributed appropriately among 142 rivers and streams that enter at the sides of the fjord. Secretary Island wind stress vectors were rotated so that winds were either directed in the up-fjord or down-fjord direction. This is appropriate since the near-vertical sides of the fjord orographically steer the true winds.

An important feature of the model is that it does not utilize a turbulence closure scheme; rather, it relies upon very high vertical resolution over the top 20 m of the water-column. A consequence of this configuration is the necessity of defining a vertical mixing scheme. The approach taken here was to try various schemes proposed in the literature and run the model

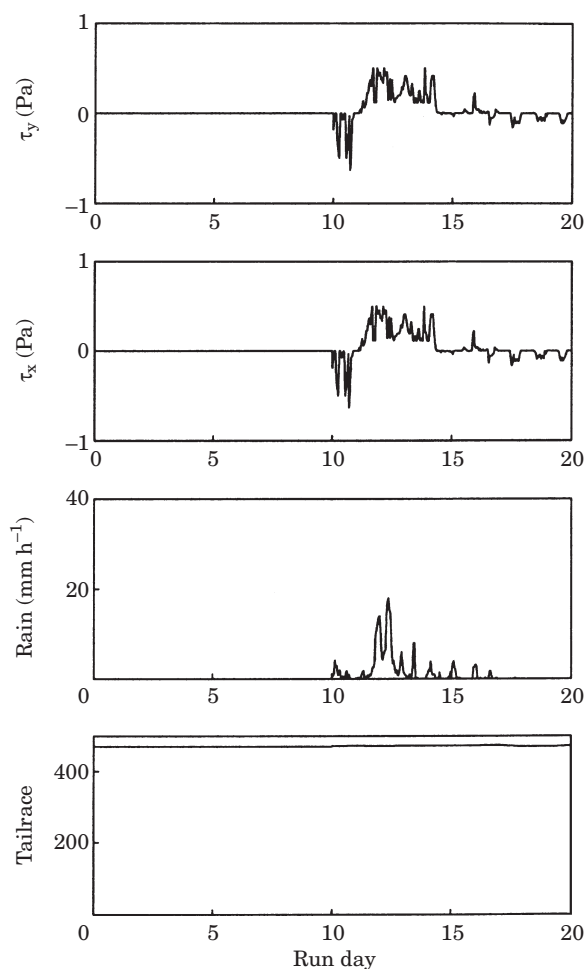


FIGURE 17. Wind stress and rainfall data used to force the numerical model.

with real winds and rain and compare the near-surface stratification with the measured stratification from the data acquired from the moorings. Best results were achieved using the scheme of Pacanowski and Philander (1981). Nunes Vaz and Simpson (1994) also found that this scheme performed better than similar schemes.

The results of two model runs are presented here. Firstly a simulation of the strong wind and rain event commencing on day 295 is shown and compared to the data. The second run shows the response to the real rain event acting in isolation. Both of the runs simulate a 20 day period. During the first 10 days the model is forced only by the input of freshwater from the tailrace ($470 \text{ m}^3 \text{ s}^{-1}$). The real winds and rain data are introduced on day 10 and the model then simulates the response to 10 days of real winds and rain.

The wind stress and rainfall input for the first model run is presented in Figure 17. A comparison of the

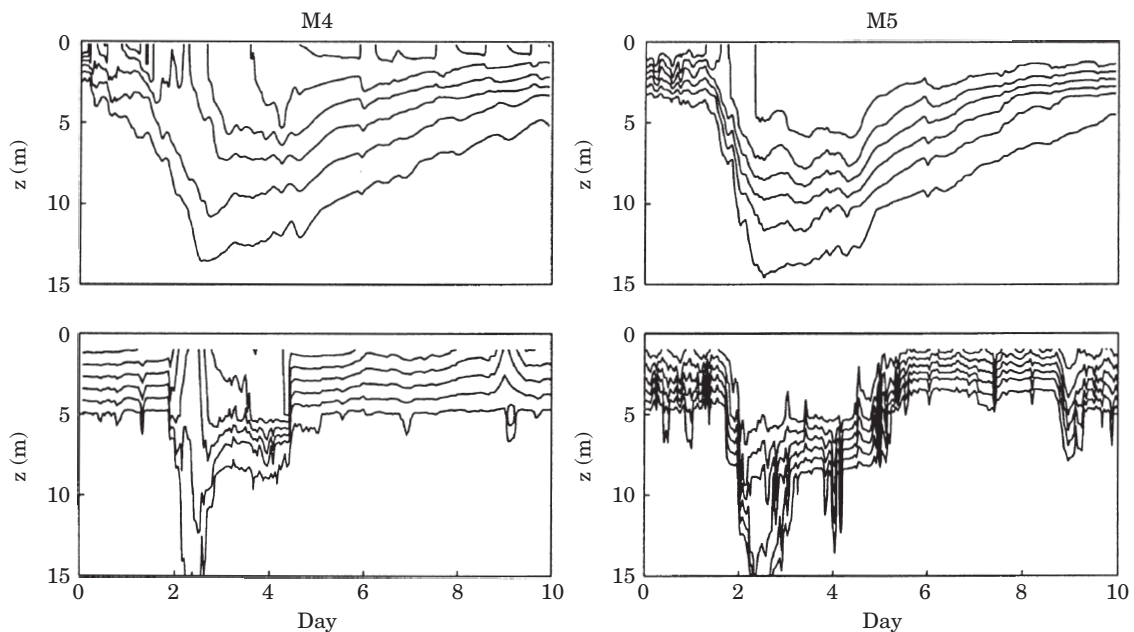


FIGURE 18. Time series of simulated (top frames) and measured (lower frames) near-surface salinities at the locations of the moorings for the first simulation. The contour interval is 5. The lower continuous contour is 30 for both the simulated and observed time series.

vertical salinity structure with the data at M4 and M5 are shown in Figure 18. The plots show only the final 10 days of the simulations when the model was forced by both the wind and rain data. The agreement between the observed and simulated salinity structure is good. The model reproduces the basic behaviour of the LSL including the significant deepening that occurs on day 2 in Figure 18. The poorest agreement between the simulated and observed structure is after the strong forcing has abated (from day 5 in Figure 18). Clearly the model has difficulty in restratifying quickly enough. This is discussed in more detail later.

The good agreement between the simulation and observations at M5 in Deep Cove was unexpected since the model laterally mixes the tailrace discharge over the whole width of Deep Cove (4 grid points). In reality the tailrace forms a meandering jet around 1–2 grid cells wide. The M5 mooring is generally within this jet hence it was expected that agreement with the model and observations at M5 would be significantly worse than at the other locations.

Along-fjord velocity sections along the main axis of Doubtful Sound (Figure 16) are presented in Figure 19. The fjord entrance is at the 6 km mark and Deep Cove branches off 38 km along these sections. The dashed contours represent outflowing currents and the solid contour show up-fjord currents. Only days 10 to 15 are shown here since the strong forcing

events occurred on these days. The velocity section at day 10 represents the standard estuarine circulation case since the only forcing prior to this day was from the tailrace discharge. On this day we see maximum outflowing currents of 8.7 cm s^{-1} . By contrast the surface currents on day 12 reverse and flow upstream into the fjord in response to the strong up-fjord wind stress (Figure 19; solid lines in top 10 m). The pressure field on this day shows sea surface elevations of 160 mm above the mean sea level at the head of the fjord, significantly greater than the elevation simulated prior to the onset of the wind stress (Figure 20). The velocity fields on days 13 and 14 show a seiche of the surface currents in response to the forcing. A strong outflowing surface current is evident on day 15 (117 cm s^{-1}) after the abatement of the wind and rain. Hence, the along-fjord velocity and pressure sections reveal that a storm surge develops in response to the up-fjord directed winds. The wind driven surface currents are strong enough to overcome the down-fjord directed flow of freshwater.

Evidence of this ‘piling up’ of low salinity water at the head of the fjord may also be seen in the time series of *EFD* (Figure 9). The *EFD* estimates at M5 show an increase in the volume of freshwater at the head of the fjord and corresponding deepening of freshwater isohalines (Figure 3). In addition, the maximum values of the *EFD* at M4 and M3 lag the wind stress and also the *EFD* at M5. This agrees with

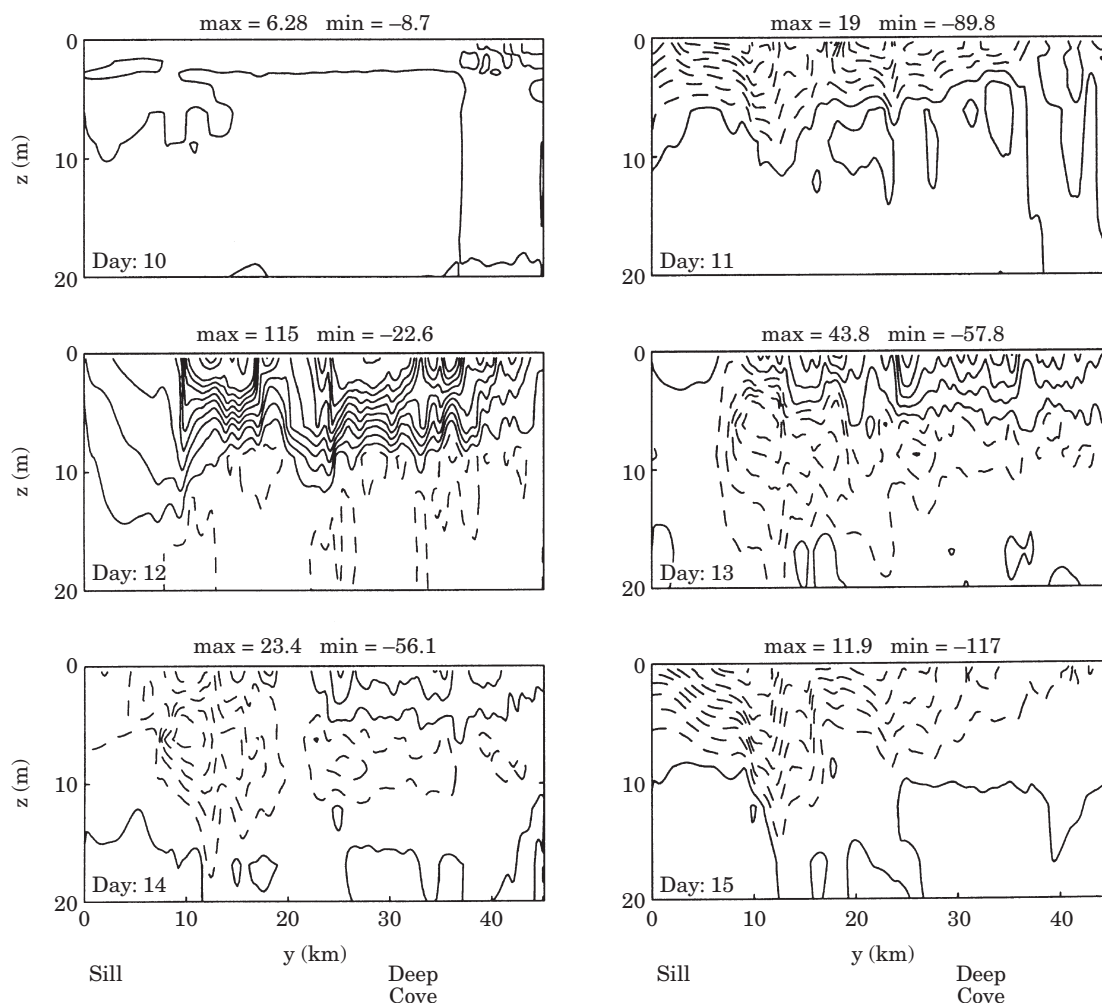


FIGURE 19. Along-fjord velocity (cm s^{-1}) sections along the main axis of Doubtful Sound for the first simulation. Dashed (solid) contours show outflowing (inflowing) currents. The contour interval is 10 cm s^{-1} . Maximum and minimum values are also shown.

the simulations that show the runout of freshwater after the wind stress has abated. The storm surge at the head of the fjord also has a critical influence on the stratification and results in both strong temporal lags and spatial differences in the response of the near-surface stratification. This result is significant as it suggests that control over the near-surface stratification during these events is dominated by the development and relaxation of the storm surge, rather than simple additional runout of fresh water in response to increased rainfall as previously believed. Hence the wind stress plays a dual role in determining the stratification through the combined action of altering the horizontal advection and through vertical mixing.

The second run simulated the response to rainfall only. Hence, the model was run with only the rain shown in Figure 17. The time series of near-surface salinities at M4 and M5 are shown in Figure 21.

Contours in these figures are the same as in Figure 17. Evidence of a pulse of low salinity water can be traced through M5 during day 12 and through M4 during day 13. Interestingly, the model suggests that the rain acting in isolation deepened the LSL only by around 2–3 m although the stratification did tighten up and became more pronounced. The along-fjord velocity fields (not shown) revealed that the pulse of low salinity water advected downstream at a speed of around 20 cm s^{-1} . This value lies between the observed phase speed of an evolving LSL in Doubtful Sound ($\sim 5 \text{ cm s}^{-1}$; G. Allen, unpubl. data) and the theoretical phase speed of a shallow internal gravity wave (50 cm s^{-1}). This speed of the buoyant flow is important as the work presented here demonstrates that the advection of buoyancy is a dominant term in controlling the stratification. Clearly more model development work is required and this is currently

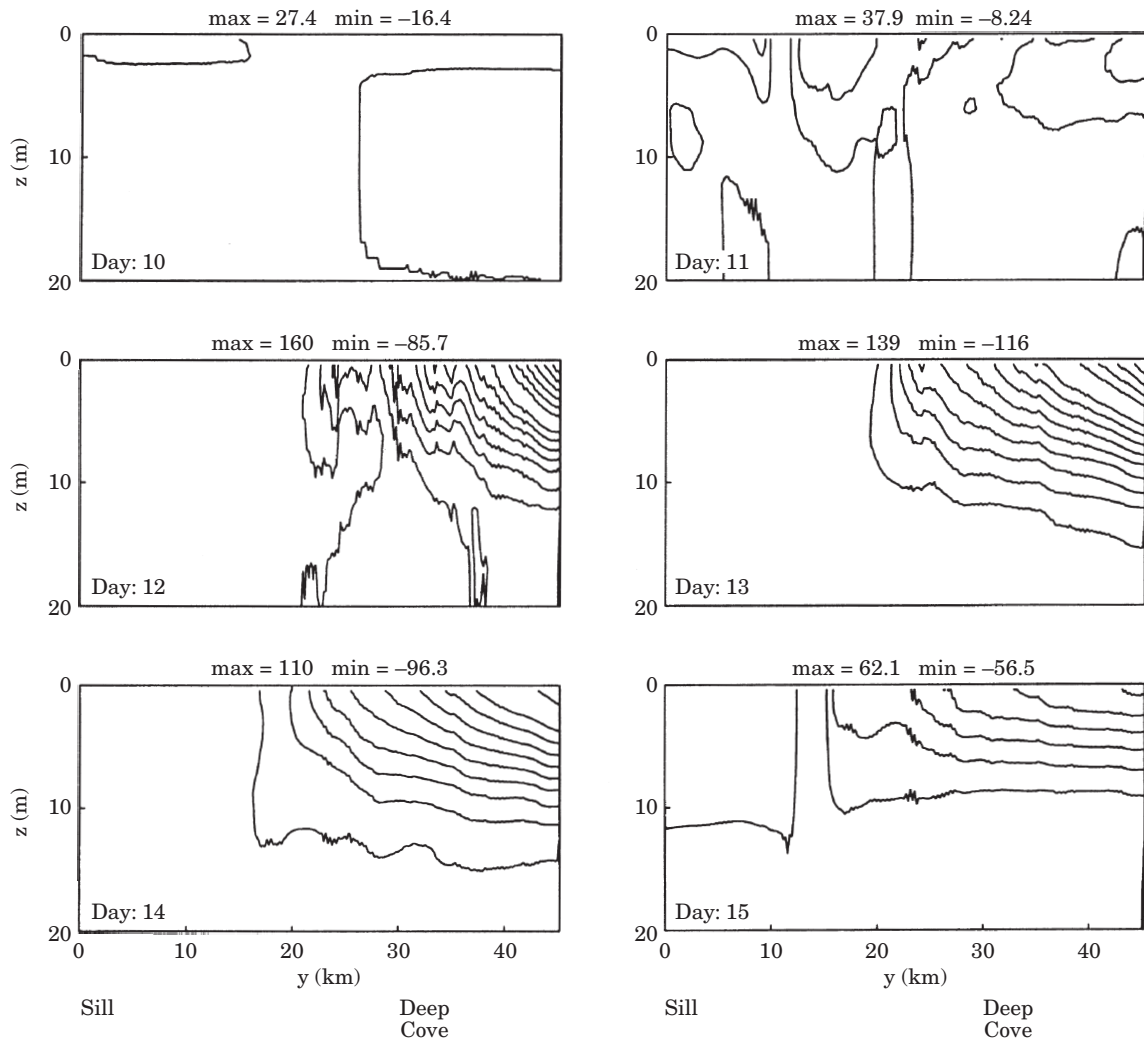


FIGURE 20. Along-fjord sections of equivalent free surface elevation (mm) along the main axis of Doubtful Sound for the first simulation. Dashed (solid) contours show negative values that show sea level depressions. The contour interval is 10 mm. Maximum and minimum values are also shown.

underway. However, the simulations performed here achieved the aim of the numerical work in that they have elucidated the roles that the natural forcing processes play in maintaining the stratification.

Summary and concluding remarks

Shallow estuaries with large intertidal volumes are often subjected to enhanced vertical mixing through the action of tidally forced bottom boundary stresses. By contrast, fjords represent a special case of estuaries since intertidal volumes are generally small by comparison with total volumes. Hence, tidal mixing in fjords is usually very small except over shallow sills. In addition, fjords are generally located in regions subjected to high rates of precipitation. The combination

of low tidal mixing and availability of buoyancy from runoff can act to maintain the near-surface stratification in the form of a robust LSL. The year-round or seasonal existence of an LSL has been shown to be a controlling factor in abundance and distribution of benthic rock wall biota in some fjords. This has particularly been the case in Doubtful Sound, a fjord that features a very robust LSL and possibly unique rock wall assemblages. However, as discussed in the introduction, no studies have focused on the structure and variability of an LSL itself.

The principal aims of the work presented here were to examine the variability in the Doubtful Sound LSL and determine how the LSL responds to the natural forcing by the wind stress and rainfall. The data shown in Figures 3–5 revealed the existence of large

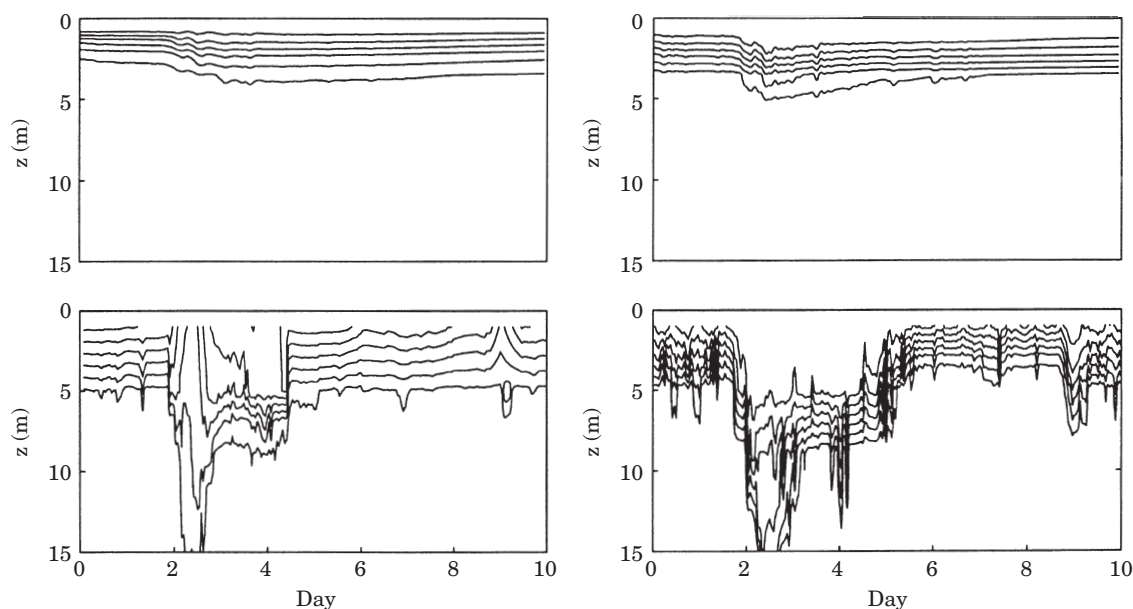


FIGURE 21. Time series of simulated (top frames) and measured (lower frames) near-surface salinities at the locations of moorings M4 and M5 for the second simulation.

perturbations in the salinity field in the upper water column that occurred concurrently with strong wind and rain events. The analyses in the frequency domain confirmed the strong coupling between the wind and rainfall in particular frequency bands. The spectral analyses also revealed strong relationships between the stratification indices φ and EFD , and both the wind stress and rainfall independently although these analyses did not adequately resolve these responses. The frequency domain analyses also revealed significant phase lags particularly between the EFD and the rainfall. A possible explanation for these lags was that freshwater ‘piles up’ at the head of the fjord during strong wind events. Since all of the strong wind events were up-fjord directed, the accumulation of freshwater would be in the form of a storm surge. However, the frequency domain analyses failed to conclusively separate the response to strong wind events from the response to strong rain events.

An analytical vertical mixing model describing temporal variability in the potential energy anomaly φ was then applied to Deep Cove. The hindcasted rate of change of φ from the model was in reasonable agreement with the observations during periods of large perturbations in the stratification. During these periods the model suggested that the dominant dynamical balances were between the wind stress mixing term and an entrainment term. Stratification was restabilized after the abatement of the wind stress by the horizontal buoyancy flux. During periods of low forcing the agreement between the model and the

observations was poorer. In addition, the role of the rainfall was not clearly established in this model since the effect of the rainfall was partitioned into a surface buoyancy term and the incoming flux of buoyancy in the differential advection term. Perhaps the most interesting outcome from the application of the analytical model was the delay in the activation of the horizontal buoyancy flux term in Deep Cove. This was unexpected although the frequency domain analysis also alluded to this result. This delay in the activation of the horizontal buoyancy flux term until after strong wind events suggested that storm surges develop at the head of the fjord during strong wind events.

A numerical model was then used to further elucidate the roles of the natural forcing processes. As highlighted previously, the model was not used here to identify aspects of the circulation with Doubtful Sound, rather, the model was used purely to attempt to elucidate aspects of the response of the near-surface stratification to the wind stress and rainfall. The agreement between the modelled and observed salinity structure was good and the simulations clearly revealed the development of storm surges during strong up-fjord wind events. As highlighted previously, this result is significant since the wind stress has not previously been shown to be a dominant forcing process in the New Zealand fjords although the wind stress has been shown to be an important forcing process in Scandinavian fjords (Leth, 1995). The development of the storm surge revealed in the

model also explains the observed phase lags between the rain and *EFD* and the rain and ϕ in addition to the delay in the activation of the horizontal buoyancy flux in Deep Cove.

A surprising outcome from the numerical simulations was that response of the LSL to high rainfall alone is minimal by comparison with the response to wind events. Unfortunately all of the strong rainfall events coincided with strong wind events during the observation period, hence inspection of the data cannot directly verify this result.

The work presented here has important implications for the management of the fjord and the power station since the response of the fjord to natural forcing has been revealed. The next step is to determine the response to fluctuations in the tailrace discharge, and this is currently being investigated. However, it has been shown here that natural forcing processes, in particular strong wind events, can introduce a significant amount of deepening of the LSL. In addition, the response of the LSL in the form of a storm surge ensures that the time dependent structure of the LSL at the different locations within the fjord will vary. This result is also important as it suggests that knowledge of the behaviour of the LSL in one location within the fjord cannot necessarily be directly applied to other sites within Doubtful or Thompson sounds.

Acknowledgements

The authors wish to thank Meridian Energy for their participation in this project and the National Institute for Water and Atmosphere Ltd. New Zealand for providing the Secretary Island wind data. This project would also not have been possible without the commitment of Philip Mladenov. We also thank Paul Meredith, Chris Spiers, Daryl Coup and all other members of the Department of Marine Science who assisted in the maintenance of the moorings.

References

- Baker, P. & Pond, S. 1995 The low-frequency residual circulation in Knight Inlet, British Columbia. *Journal of Physical Oceanography* **25**, 747–763.
- Bowman, M. J. 1978 Spreading and mixing of the Hudson River effluent into the New York Bight. In *Hydrodynamics of Estuaries and Fjords* (Nihoul, J. C., ed.), Oceanography Series No. 23, Elsevier, Amsterdam, pp. 373–386.
- Bowman, M. J., Dietrich, D. E. & Mladenov, P. 1999 Predictions of circulation and mixing in Doubtful Sound, arising from variations in runoff and discharge from the Manapouri power station. In *Coastal Ocean Prediction, Coastal and Estuarine Studies* no. 56. American Geophysical Union, pp. 59–76.
- Dietrich, D. E., Marietta, M. G. & Roache, P. J. 1987 An ocean modeling system with turbulent boundary layers and topography: numerical description. *International Journal of Numerics in Fluids* **7**, 833–855.
- Edwards, A. & Edelsten, D. J. 1977 Deep water renewal of Loch Etive: a three basin Scottish fjord. *Estuarine, Coastal and Shelf Science* **5**, 575–595.
- Farmer, D. M. & Freeland, H. J. 1983 The physical oceanography of fjords. *Progress in Oceanography* **12**, 159–219.
- Gade, H. G. 1973 Deep water exchange in a sill fjord. A stochastic process. *Journal of Physical Oceanography* **3**, 213–219.
- Grange, K. R. & Singleton, R. J. 1988 Population structure of black coral, *Antiphees aperta*, in the southern fjords of New Zealand. *New Zealand Journal of Zoology* **15**, 481–489.
- Kaartvedt, S. & Svendsen, H. 1990 Impact of freshwater runoff on physical oceanography and plankton distribution in a western Norwegian fjord: an experiment with a controlled discharge from a hydroelectric power plant. *Estuarine, Coastal and Shelf Science* **31**, 381–395.
- Large, W. S. & Pond, S. 1981 Open ocean momentum flux measurements in moderate to strong winds. *Journal of Physical Oceanography* **11**, 324–336.
- Leth, O. K. 1995 A study on the effect of local wind dynamics of the upper layer in the inner part of Malangen. In *Ecology of Fjords and Coastal Waters* (Skjoldal, H. R., Hopkins, K. E., Erikstad, K. E. & Leinaas, H. P., eds), Elsevier, Amsterdam, pp. 185–194.
- McCully, D. R., Vennel, R. & Maldon, P. V. 1995 Hydrology of a New Zealand fjord. *Recent Advances in Marine Science and Technology '94*. Bellwood, O., Choat, H. & Saxena, N. eds), pp. 263–271.
- Nunes Vaz, R. A., Lennon, G. W. & de Silva Samarasinghe, J. R. 1989 The negative role of turbulence in estuarine mass transport. *Estuarine, Coastal and Shelf Science* **28**, 361–377.
- Nunes Vaz, R. A. & Simpson, J. H. 1994 Turbulence closure modeling of estuarine stratification. *Journal of Geophysical Research* **99**, 16 143–16 160.
- Pacanowski, R. C. & Philander, S. G. H. 1981 Parameterisation of vertical mixing in numerical models of tropical oceans. *Journal of Physical Oceanography* **11**, 1443–1451.
- Rasmussen, B. 1997 The near-surface horizontal buoyancy flux in a highly stratified region, Kattegat. *Estuarine, Coastal and Shelf Science* **45**, 405–414.
- Richardson, K. & Christoffersen, A. 1991 Seasonal distribution and production of phytoplankton in the southern Kattegat. *Marine Ecology Progress Series* **78**, 217–227.
- Simpson, J. H., Allen, C. M. & Morris, N. C. G. 1978 Fronts on the continental shelf. *Journal of Geophysical Research* **83**, 4607–4614.
- Simpson, J. H. & Bowers, D. 1981 Models of stratification and frontal movement in shelf seas. *Deep-Sea Research* **28**, 727–738.
- Smith, F. & Witman, J. D. 1999 Species diversity in subtidal landscapes: maintenance by physical processes and larval recruitment. *Ecology* **80**, 51–69.
- Stanton, B. R. & Pickard, G. L. 1981 Physical oceanography of the New Zealand fjords. *New Zealand Oceanographic Institute Memoir* **88**, 3–37.
- Stanton, B. R. 1984 Some oceanographic observations in the New Zealand fjords. *Estuarine, Coastal and Shelf Science* **19**, 89–104.
- Stanton, B. R. 1986 Winter oceanographic observations in some New Zealand fjords. *New Zealand Journal of Marine and Freshwater Research* **20**, 299–314.
- Witman, J. D. & Grange, K. R. 1998 Links between rain, salinity and predation in a rocky subtidal community. *Ecology* **79**, 2429–2447.